

**OPTICAL AND ELECTRICAL PROPERTIES OF EPITAXIAL SILVER
FILMS GROWN ON SILICON**

by

Jinxuan Wu

B.S. in Electronic and Information Science and Technology, Peking University, 2009

Submitted to the Graduate Faculty of
Swanson School of Engineering in partial fulfillment
of the requirements for the degree of
Master of Science in Electrical Engineering

University of Pittsburgh

2012

UNIVERSITY OF PITTSBURGH
SWANSON SCHOOL OF ENGINEERING

This thesis was presented

by

Jinxuan Wu

It was defended on

March 28, 2012

and approved by

Mahmoud El Nokali, PhD, Associate Professor, Department of Electrical and Computer
Engineering

Yiran Chen, PhD, Assistant Professor, Department of Electrical and Computer Engineering

Thesis Advisor: Hong Koo Kim, PhD, Professor, Department of Electrical and Computer
Engineering

Copyright © by Jinxuan Wu

2012

**OPTICAL AND ELECTRICAL PROPERTIES OF EPITAXIAL SILVER FILMS
GROWN ON SILICON**

Jinxuan Wu, M. S.

University of Pittsburgh, 2012

Light absorption and photocarrier transport are commonly important processes of photovoltaic energy conversion. In this thesis we have explored nanostructured metal contacts on semiconductor surfaces that may provide a synergistic improvement of these fundamental processes therefore the overall cell efficiency. This research is based on the previous work at Prof. Kim's lab: a simple thin-film deposition process was developed that can grow nanostructured metal films on native-oxide covered silicon surface [Phys Rev B 75, 205306 (2007); J Appl Phys 103, 103507 (2008)]. This thin-film process involves the Stranski-Krastanov growth mode, that is, growth of a thin wetting layer followed by formation of 3D nano-islands, both in good epitaxial relationship with Si substrate. The process temperature is significantly lower than that of conventional silver thick-film process. In this study we have investigated the potential to use the nanostructured epitaxial metal contacts on Si as a means to achieve low contact resistivity and also to enhance light trapping/coupling. We characterized the optical reflectance at various incident angles. The film and contact resistivities of Ag on Si were also characterized for various different film thicknesses.

TABLE OF CONTENTS

PREFACE.....	XI
1.0 INTRODUCTION.....	1
2.0 THEORY	3
2.1 METAL-SEMICONDUCTOR CONTACT	3
2.2 CONTACT RESISTANCE AND RESISTIVITY	8
3.0 OPTICAL PROPERTIES CHARACTERIZATION.....	14
3.1 EXPERIMENTAL SETUP.....	14
3.1.1 Epitaxial Ag preparation	14
3.1.2 Angular dependence of reflection characterization	16
3.2 EXPERIMENTAL RESULT.....	18
3.2.1 Results of bare crystalline silicon substrate	18
3.2.2 Results of epitaxial Ag covered silicon substrate.....	21
4.0 ELECTRICAL PROPERTIES CHARACTERIZATION.....	30
4.1 EXPERIMENTAL SETUP.....	30
4.1.1 Epitaxial Ag preparation	30
4.1.2 Contact resistivity characterization using TLM analysis	36
4.2 EXPERIMENT RESULT AND DISCUSSION	37
4.2.1 Epitaxial Ag-Si contact resistivity	37

4.2.1.1	Ag samples using mm scale pattern on medium doped substrate ..	37
4.2.1.2	Ag samples using μm scale pattern on medium doped substrate ...	40
4.2.1.3	Ag samples using mm scale pattern on highly doped substrate	43
4.2.2	Epitaxial Ag resistivity	48
5.0	SUMMARY	56
	BIBLIOGRAPHY	58

LIST OF TABLES

Table 3.1 Sputtering condition of samples for optical characterization	15
Table 4.1 Sputtering Condition of samples for electrical characterization.....	31
Table 4.2 Photolithography Condition for TLM patterning	35
Table 4.3 Thermal Evaporation Condition for Al deposition.....	35
Table 4.4 Result of contact resistivity characterization for epitaxial Ag-Si and Al-Si reference (shadow mask, mm scale, substrate: medium doped).....	38
Table 4.5 Result of contact resistivity characterization for epitaxial Ag-Si and Al-Si reference (photolithography mask, μm scale, substrate: medium doped)	41
Table 4.6 Result of contact resistivity characterization for epitaxial Ag-Si and Al-Si reference (photolithography mask, mm(Ag)/ μm (Al) scale, substrate: highly doped).....	44
Table 4.7 Summary of experiment result for epitaxial Ag film on Si	45
Table 4.8 Result of substrate sheet resistance characterization for epitaxial Ag-Si (shadow mask, mm scale, substrate: medium doped).....	50
Table 4.9 Result of substrate sheet resistance characterization for epitaxial Ag-Si (photolithography μm scale, substrate: medium doped).....	51
Table 4.10 Result of sheet resistance for epitaxial Ag covered Si for film thickness effect (shadow mask, mm scale, substrate: medium doped).....	52
Table 4.11 Summary of experiment result about epitaxial Ag film resistivity on Si	54

LIST OF FIGURES

Figure 2.1 Energy band diagram for metal-semiconductor contacts explained with simple Schottky model. Low barrier height diagrams: a) before contacting, b) after contacting in equilibrium. High barrier height diagrams: c) before contacting, d) after contacting in equilibrium.....	5
Figure 2.2 The effect of substrate doping level on barrier height and width. The barrier width decreased when doping level increased: from a) low doping, b) medium doping to c) highly doping. The barrier also reduced from ϕ_B to ϕ'_B because image force lower the barrier.	7
Figure 2.3 Illustration of TLM analysis. a) The pattern of electrodes to make TLM measurement b) the R-L curve to obtain parameters for contact resistivity calculation.....	12
Figure 2.4 a) The actual condition of current flowing between electrodes. b) A TLM equivalent circuit for current flow between electrodes.	13
Figure 3.1 Scheme of optical characterize system setup to measure angular dependence of reflection	17
Figure 3.2 Angel-dependent reflectance of crystalline silicon at 633nm wavelength.....	20
Figure 3.3 Angle-dependent reflectance of crystalline silicon with 7 nm epitaxial Ag covered at 633 nm wavelength.....	24
Figure 3.4 Angle-dependent reflectance of crystalline silicon with 10 nm epitaxial Ag covered at 633 nm wavelength.....	24
Figure 3.5 Angle-dependent reflectance of crystalline silicon with 11 nm epitaxial Ag covered at 633 nm wavelength.....	25
Figure 3.6 Angle-dependent reflectance of crystalline silicon with 13 nm epitaxial Ag covered at 633 nm wavelength.....	25
Figure 3.7 Angle-dependent reflectance of crystalline silicon with 15 nm epitaxial Ag covered at 633 nm wavelength.....	26

Figure 3.8 Angle-dependent reflectance of crystalline silicon with 20 nm epitaxial Ag covered at 633 nm wavelength.....	26
Figure 3.9 Angle-dependent reflectance of crystalline silicon with 40 nm epitaxial Ag covered at 633 nm wavelength.....	27
Figure 3.10 Comparison of angle-dependent average reflectance of crystalline silicon with epitaxial Ag (0-15 nm) covered at 633 nm wavelength.....	27
Figure 3.11 Comparison of angle-dependent average reflectance of crystalline silicon with epitaxial Ag (0-40 nm) covered at 633 nm wavelength.....	28
Figure 3.12 SEM image of epitaxial Ag films on Si deposit for (a) 40 s, (b) 50 s and (c) 60 s [3].	29
Figure 4.1 Structure of prepared samples in electrical characterization. a) Discrete epitaxial Ag sample is for study of contact resistivity and b) continuous sample is for study of epitaxial Ag conductivity.....	32
Figure 4.2 mask pattern design. a) mm scale mask (available in shadow mask and lithography mask). b) μm scale mask (available in lithography mask only).....	33
Figure 4.3 R-L curves: a, b) Ag-Si samples patterned by shadow mask with mm scale pattern and discrete epitaxial Ag layer. c) Al-Si samples patterned by same shadow mask. d) Al-Si samples patterned by photolithography mask which has the same pattern as shadow mask used in previous samples.....	39
Figure 4.4 R-L curves: a) Ag-Si samples patterned by photolithography mask with μm scale pattern and discrete epitaxial Ag layer. b) Al-Si samples patterned by same by photolithography mask.....	42
Figure 4.5 R-L curves: Ag-Si samples patterned by shadow mask with mm scale pattern and discrete epitaxial Ag layer on highly doped substrate.....	44
Figure 4.6 Phase diagram of Ag-Si and Al-Si material system [17]	47
Figure 4.7 R-L curves: Ag-Si samples patterned by shadow mask with mm scale pattern and continuous epitaxial Ag layer on medium doped substrate.....	49
Figure 4.8 R-L curves: Ag-Si samples patterned by photolithography mask with μm scale pattern and continuous epitaxial Ag layer on medium doped substrate.....	51
Figure 4.9 Illustration of current flow between electrodes for continues epitaxial Ag films covered Si. a) Before grain shape surface formed, only sparse boundaries occur in the film b) After grain shape surface formed, the grain structure contributes to increasing the thickness of	

the film but not the current flow because boundaries of grains serve as barrier to prevent carrier transfer. 53

Figure 4.10 XPS analysis results of a Ag film sputtered for 90 s at 550°C: a) Depth profiles of Ag, O and Si, b) Depth profile of Si 2p energy spectra, c) Depth profile of O 1s energy spectra [2] 55

PREFACE

I would like to thank my advisor Prof. Hong Koo Kim for his guide and support during I studied and worked in University of Pittsburgh. From him I have obtained invaluable knowledge in both scientific and professional aspects. I believe the time I have spent with him would be extremely helpful for my future career.

I would like to thank Prof. Mahmoud El Nokali and Prof. Yiran Chen for taking their precious time to serve on my committee and their valuable comments on my thesis.

I would also like to thank my office mates in lab Dr. Dongxiao Li, Dr. Yun-Suk Jung, Siwapon Srisonphan, Myungji Kim, Zhenlv Han and I-Hung Ting for their help in study and life. Their advice and encouragement were of great help to me and I really have great time with them.

I want to show my greatest thanks to my parents and families for their selfless love and support. They have always been with me and concern about my life and future. I hope we can get together forever.

Finally I want to thank everyone who has helped me during my study in Pittsburgh. It would be hard here without their help.

1.0 INTRODUCTION

Over the past decades, epitaxial growth of metal films on Si substrates has been a widely studied topic since unique optical and electrical properties might be obtained from such material system [1]. Ag on Si is one of the most common metal-Si material systems which is nonreactive and can form a well-defined interface, which had also been extensively studied. As one among these researches, previous study of epitaxial Ag films grown on Si had been reported in our group [2] [3]. It was reported that on a native-oxide-covered Si substrate, epitaxial Ag films were grown by radio-frequency (RF) magnetron sputtering at 550°C. During deposition, native oxide on Si was removed therefore well-defined interface of Ag-Si was formed. Also, the morphology evolution was studied. From these studies we learned that our Ag-film process involved Stranski-Krastanov growth, which indicate that thin epitaxial wetting films formed in the initial film formation stage and grain structure formed later when the film thickness increased further [4]. The fabrication of this kind of films is relatively simpler than other methods of Ag growth on Si with surfaces cleaned in ultrahigh vacuum (UHV) [5], and the process temperature is significantly lower than the conventional Ag-Si annealing temperature. Thus there are several advantages of our epitaxial Ag deposition.

Still, the optical and electrical properties of our epitaxial Ag films were not characterized in previous researches, which become our primary interest in this article. In this study, we have investigated the optical as well as electrical properties of the epitaxial Ag films. In optical

characterization, we studied the effects of Ag films on angular dependence of reflection. We found that with thin epitaxial Ag coated the reflectance increased in a negligible amount. We further processed the electrical characterization on the thin epitaxial Ag films and characterized the resistivity of the epitaxial Ag films as well as the contact resistivity of the epitaxial Ag-Si. Ohmic contact, as well as compatible contact resistivity with conventional Al-Si contact, was found. Also, thin Ag film coating helped reduce the sheet resistance of the Si and we obtained the material resistivity of our Ag films.

In Chapter 2 of this thesis, we introduce and discuss the fundamental theories which support the work of the thesis, which will assist us in understanding and analyzing the experiment results. Chapter 3 is about the optical characterization experiments, which include fabrication process, the characterization system set up and results analysis of Ag films on Si. In Chapter 4, we describe the electrical characterization experiments and analyze the results. A brief summary is given in the last chapter.

2.0 THEORY

In this chapter we will discuss the fundamental principles to develop the research in this article. First we will introduce the concept of metal-semiconductor contact, and further discuss ohmic contact and Schottky contact. To characterize the metal-semiconductor contact, a typical technique called transmission line model or transfer length method (TLM) of metal-semiconductor contact, first proposed by Shockley and later developed by Berger [6] [7], has been used to determine the contact resistance and resistivity of planar metal-semiconductor contact, mostly ohmic contact. To better understand our electrical characterization, we will discuss about this TLM method and describe how to measure the contact resistance and resistivity.

2.1 METAL-SEMICONDUCTOR CONTACT

The metal-semiconductor contact is one of the oldest types of semiconductor devices. In 1930's, Schottky first developed an acceptable theory to explain the rectifying I-V properties of one kind of such devices, in which the I-V characteristics is obviously different for forward and reverse bias. Such devices are now name as Schottky-barrier devices and this type of contact is called Schottky contact. Another type of devices, which shows linear or quasi-linear I-V properties, is called ohmic contacts. Usually, the voltage drop should be small enough across the contact

compared to voltage drops across the semiconductor device. In general, ohmic contacts are preferred metal-semiconductor contact for most of the devices since they do not significantly degrade or limit the device performance.

Figure 2.1 shows the Schottky model of metal-semiconductor contact. The barrier height is given by:

$$\phi_B = \phi_M - \chi \quad (2.1-1)$$

where ϕ_B is the metal work function and χ is the semiconductor affinity, which is the energy difference between the vacuum level and the bottom of the conduction band. As shown in Figure 1, if the barrier height is low, electrons can transport through the barrier freely on both direction (from semiconductor to metal or vice versa). If the barrier height is high, electrons would need external electric field to overcome such barrier, thus perform as a rectifier. It seems that for given material system, the barrier height is nearly fixed since the metal work function and the semiconductor affinity are given. However, the dependence of ϕ_B to ϕ_M is not unity as (2.1-1) predicted but weaker [8].

To determine the barrier height, a rule of thumb is that for n-type materials the height is two-thirds of the band gap and for p-type is one-third [8]. This indicates that to select a material system with low barrier height to obtain ohmic contact is nearly impossible. As a result, we need to find out other methods to implement ohmic contact. Fortunately, several typical techniques are found to be effective to form ohmic contact.

One and maybe the most appropriate technique to form good ohmic contact is to deposit metal onto a highly doped semiconductor [9]. Although the doping of semiconductor would

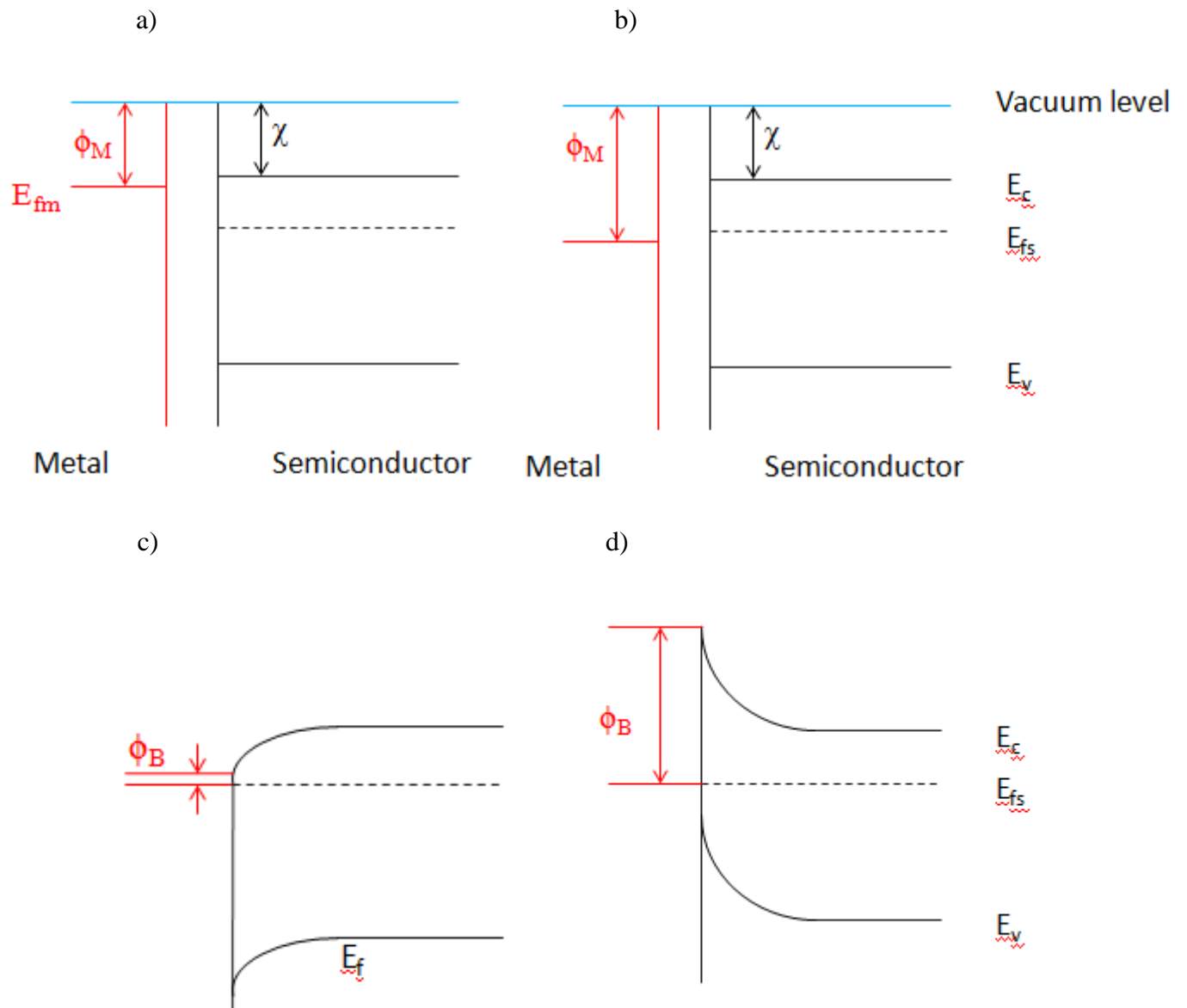


Figure 2.1 Energy band diagram for metal-semiconductor contacts explained with simple Schottky model. Low barrier height diagrams: a) before contacting, b) after contacting in equilibrium. High barrier height diagrams: c) before contacting, d) after contacting in equilibrium.

not change the barrier height, increasing the doping level of the substrate will narrow the space charge region, which allows tunneling effect of the carriers between the substrate and the metal.

Figure 2.2 illustrates the conduction mechanisms for a metal-semiconductor contact with different donor doping level. For low-doped substrate ($N_D < 10^{17} \text{ cm}^{-3}$), thermionic emission is dominant to form the current flow over the barrier and carriers need to overcome the full barrier height to across the barrier. When the doping level increased to intermediate range ($10^{17} \text{ cm}^{-3} < N_D < 10^{19} \text{ cm}^{-3}$), thermionic/field emission is dominant, which requires less energy than the barrier height for carriers to across the barrier, while image force would lower the barrier as well. The carriers are first excited by this energy to and then tunnel through the barrier which is thin enough at this place. In the highly doping range ($N_D > 10^{19} \text{ cm}^{-3}$), the barrier is thin that carriers can tunnel through the barrier at the bottom of the conduction band.

Post-deposition annealing of contact was also found to be important for ohmic contact forming. It was reported on a bulk of researched about metal-semiconductor ohmic contact forming [10] [11]. Post-deposition annealing of metal-semiconductor contact is helpful for relieving stress and reducing defects at the interface. Also, certain desirable reactions between the metal and the semiconductor might be induced during annealing, such as metal-semiconductor alloy forming. Selecting proper annealing temperature would be helpful to achieve low contact resistivity for the form ohmic contact.

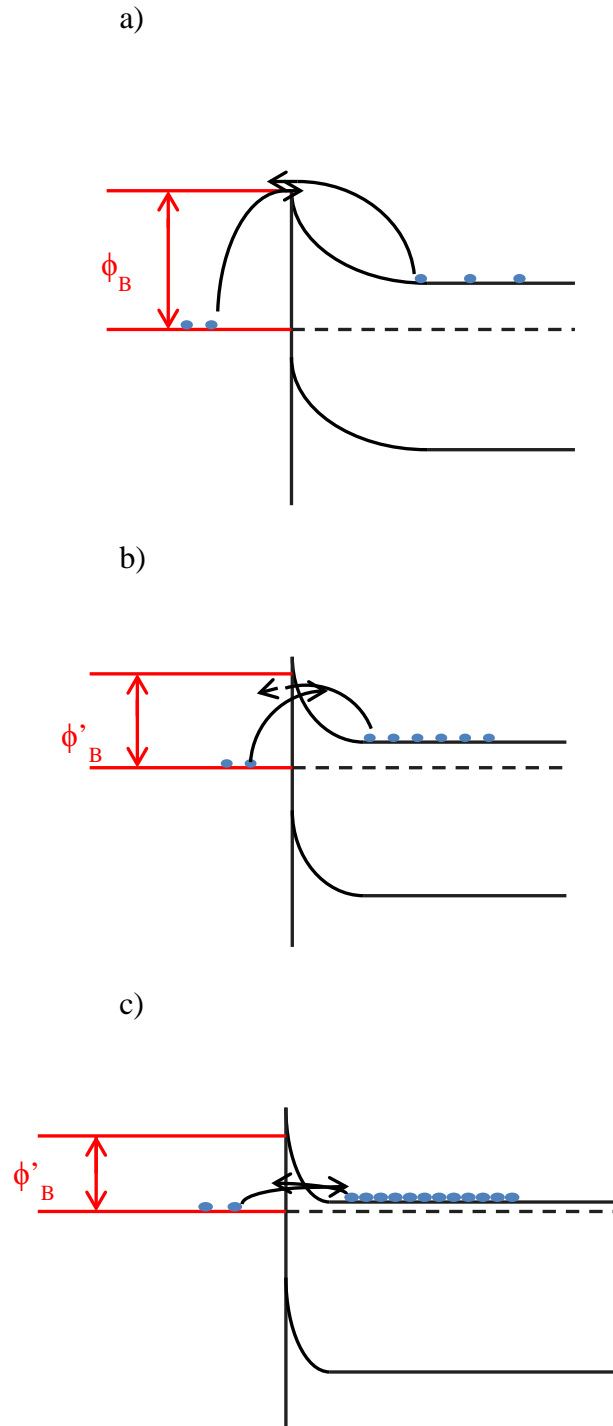


Figure 2.2 The effect of substrate doping level on barrier height and width. The barrier width decreased when doping level increased: from a) low doping, b) medium doping to c) highly doping. The barrier also reduced from ϕ_B to ϕ'_B because image force lower the barrier.

2.2 CONTACT RESISTANCE AND RESISTIVITY

Contact resistance (R_c) is defined as the resistance across the metal-semiconductor interface. Correspondingly, such resistance of a unit area is defined as contact resistivity (ρ_c). The definition of R_c and ρ_c can be describe as,

$$R_c = \left. \frac{\partial V_c}{\partial I_c} \right|_{V_c=0} \quad (2.2-1)$$

$$\rho_c = A \left. \frac{\partial V_c}{\partial I_c} \right|_{V_c=0} = \left. \frac{\partial V_c}{\partial J_c} \right|_{V_c=0} \quad (2.2-2)$$

where V_c , I_c , J_c are the voltage, current and current density across the contact interface, A is the current flow area at the interface.

To characterize the contact resistance and resistivity, TLM is a commonly used technique which works for planar contact-resistance characterization [6] [7]. The TLM structure is patterned on the samples to be tested. The pattern is a series of rectangle of width w and length d , spaced at varying distance L_1, L_2, L_3, \dots . If we measured the resistance between two of these contact with distance L_i , the resistance can be considered as the sum of two components:

$$R = 2R_c + r_s \frac{L_i}{w} \quad (2.2-3)$$

where r_s is the sheet resistance of the sample substrate between the electrodes. If we measured resistance between all pairs of adjacent electrodes and plot R versus L , then the slope of the curve would be r_s/w and the intercept would be $2R_c$. Figure 2.3 illustrates the electrode pattern and the R - L curve, with some of the parameters indicated.

From TLM structure and measurement, we can obtain some useful information, such as the contact resistance and the substrate sheet resistance. However, such information is not sufficient to characterize the contact resistivity, which is the parameter essentially represented the metal-semiconductor. We cannot decide the current flowing area across the contact. Figure 2.4 illustrate the actual condition of current flowing between electrodes, as well as a TLM equivalent circuit. We assumed that the current flows mainly through thickness h and the current is evenly distributed. Thus, in the region that $0 \leq x \leq d$, we have following equations [12]:

$$dV(x) = -I(x)dR = -I(x)\frac{R_s dx}{w} \quad (2.2-4)$$

$$dI(x) = V_c - V(x)\frac{wdx}{\rho_c} \quad (2.2-5)$$

where V_c is the voltage applied on the end electrode, R_s is the sheet resistance of the semiconductor under the electrode. Substitute (2.2-5) to (2.2-4) and we have:

$$\frac{d^2V(x)}{dx^2} - \frac{R_s}{\rho_c} = -\frac{R_s}{\rho_c}V_c \quad (2.2-6)$$

This is a second-order differential equation which can be solved by Laplace transform. After Laplace transform $V(x)$ become $F(s)$ and (2.2-6) become:

$$s^2F(s) - sV(0) - V'(0) - \frac{R_s}{\rho_c}F(s) = -\frac{R_sV_c}{\rho_c s} \quad (2.2-7)$$

$$F(s) = \frac{sV(0) + V'(0)}{s^2 - \frac{R_s}{\rho_c}} - \frac{V_c \frac{R_s}{\rho_c}}{s(s^2 - \frac{R_s}{\rho_c})} = \frac{sV(0) + V'(0)}{s^2 - \frac{R_s}{\rho_c}} + \frac{V_c}{s} - \frac{sV_c}{s^2 - \frac{R_s}{\rho_c}} \quad (2.2-8)$$

After inverse Laplace transform, (2.2-8) become:

$$V(x) = V(0) \cosh \frac{x}{L_T} + \frac{V'(0)}{k} \sinh \frac{x}{L_T} + V_c - V_c \cosh \frac{x}{L_T} \quad (2.2-9)$$

where $L_T = \sqrt{\rho_c / R_s}$. Substitute (2.2-4) to (2.2-9) with $V'(x) = dV(x) / dx$:

$$V(x) = V(0) \cosh \frac{x}{L_T} - \frac{I(0)R_s L_T}{w} \sinh \frac{x}{L_T} + V_c - V_c \cosh \frac{x}{L_T} \quad (2.2-10)$$

At the end of the electrode ($x = d$), $I(d)=0$, from (2.2-4),(2.2-10):

$$0 = \frac{dV(x)}{dx} = \frac{V(0)}{L_T} \sinh \frac{d}{L_T} - \frac{R_s I(0)}{w} \cosh \frac{d}{L_T} - \frac{V_c}{L_T} \sinh \frac{d}{L_T} \quad (2.2-11)$$

The definition of contact resistance R_c is:

$$R_c = \frac{V(0) - V_c}{I(0)} \quad (2.2-12)$$

Substitute (2.2-11) to (2.2-12):

$$R_c = \frac{R_s L_T}{w} \coth \frac{d}{L_T} \quad (2.2-13)$$

If $\frac{d}{L_T} > 1.2$, $\coth \frac{d}{L_T} \approx 1$, then:

$$R_c = \frac{R_s L_T}{w} = \frac{\rho_c}{L_T w} \quad (2.2-14)$$

$$L_T = \frac{R_c w}{R_s} = \frac{R_c}{k} \quad (2.2-15)$$

where R_c and k can be obtained from R-L curve. Here we assume that $k = r_s / w \approx R_s / w$. This represents the case that electrode is a long contact that current transfer only near the edge. This condition is stand for most of the case. However, if the electrode is not long enough, we have

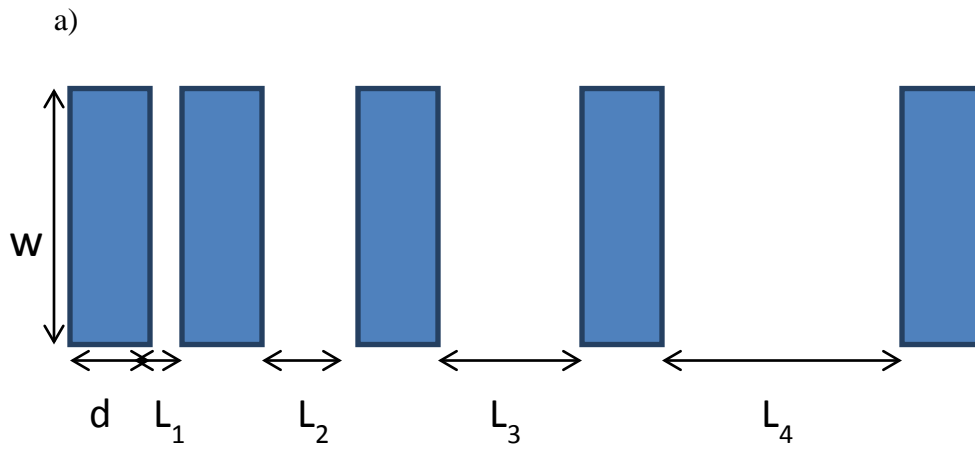
that $\frac{d}{L_T} \coth \frac{d}{L_T} \approx 1$, then

$$R_c = \frac{\rho_c}{dw} \frac{d}{L_T} \coth \frac{d}{L_T} \approx \frac{\rho_c}{dw} \quad (2.2.16)$$

Notice that we can use (2.2-15) to decide which formula we can use by deciding whether

$$\frac{d}{L_T} > 1.2.$$

One major approximation here is we assume that the substrate sheet resistance r_s is equal to the sheet resistance of substrate underneath the electrodes R_s . However, this might not be true according to the research of G.K. Reeves and H. B. Harrison [13]. Their results indicate that $R_s > r_s$ and under certain condition the difference might be more than one order of magnitude. This might because during metallization metal atoms diffused into substrate. For thin substrate such diffusion might change obviously the substrate resistivity. However, for most of the case, such approximation is acceptable especially when the substrate is relatively thick.



b)

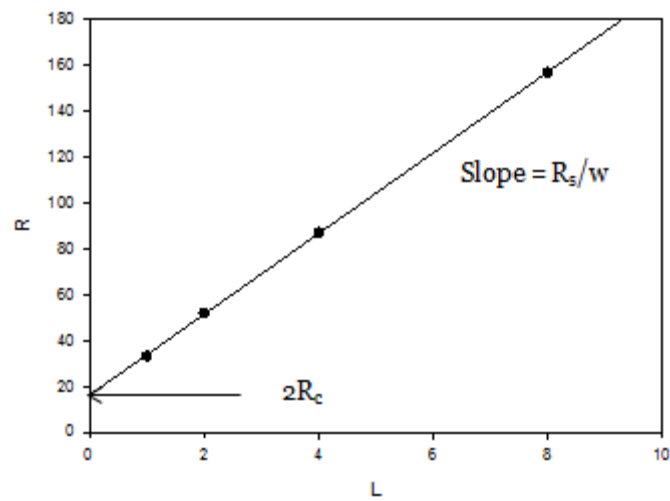


Figure 2.3 Illustration of TLM analysis. a) The pattern of electrodes to make TLM measurement
 b) the R-L curve to obtain parameters for contact resistivity calculation.

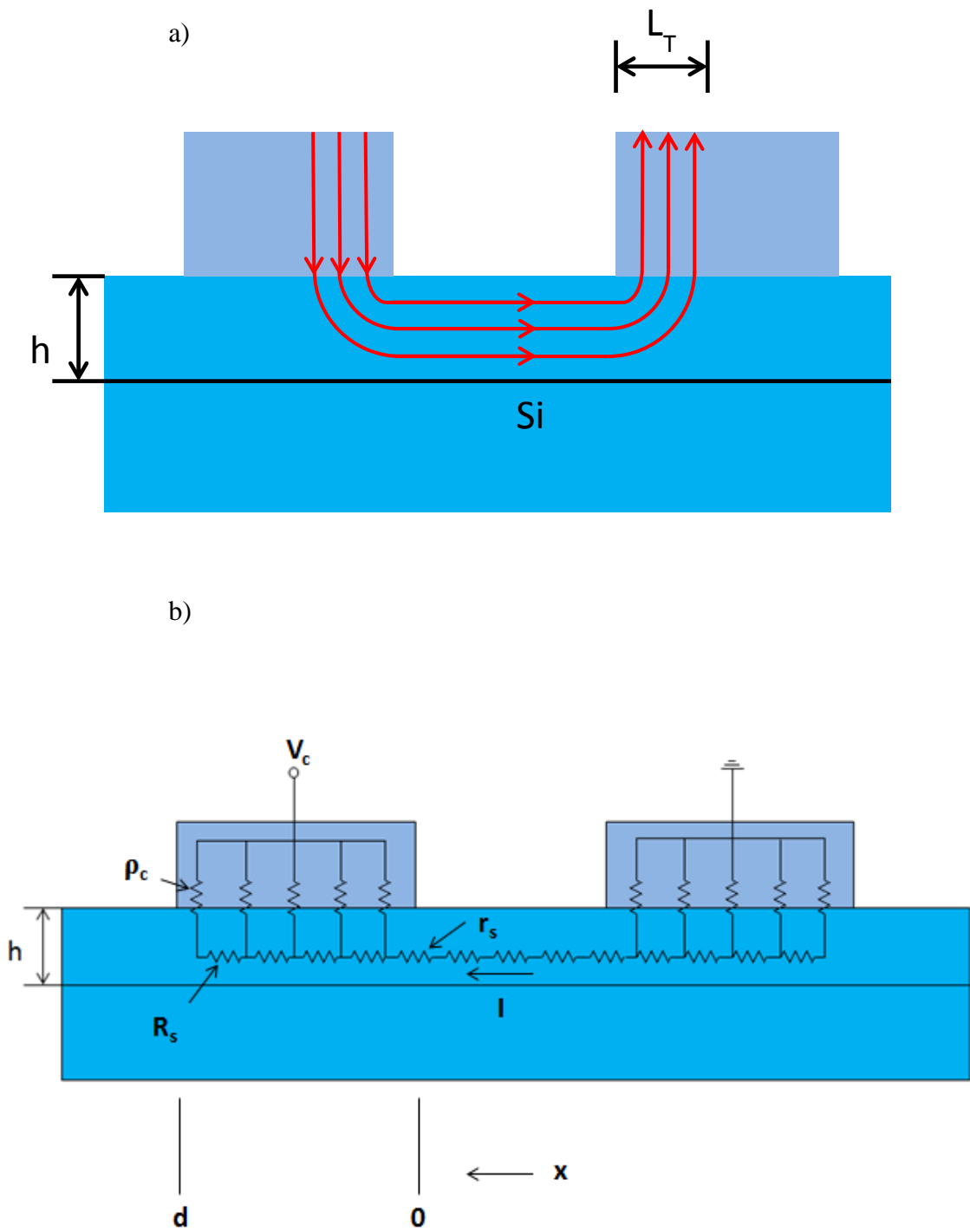


Figure 2.4 a) The actual condition of current flowing between electrodes. b) A TLM equivalent circuit for current flow between electrodes.

3.0 OPTICAL PROPERTIES CHARACTERIZATION

Optical property is a key aspect in some applications of thin film. For example, Photo-Voltaic applications require low reflectance at the surface to achieve high light trapping in the devices, which can effectively increase the efficiency of devices. Typically, we need to study the optical properties to decide whether such material can be used on certain devices and to optimize the film parameters. In this chapter we will characterize the optical properties of our epitaxial grown Ag. We will first describe the experiment setup, such as the fabrication process of epitaxial Ag and the characterization system. After that we will present and analyze our results.

3.1 EXPERIMENTAL SETUP

3.1.1 Epitaxial Ag preparation

A p-type Si (001) wafer (substrate resistivity: 10 ohm-cm) was cut into 2 cm by 2 cm approximately for deposition substrate. The Si wafer was cleaned with solvents (acetone, and methanol for 10 min respectively) in an ultrasonic bath. After ultrasonic rinse, the sample was transferred into deionized (DI) water and rinsed for 2 min. After all, it is blown dry with nitrogen gas. The purpose of this cleaning was to remove organic contamination but remain the native

oxide on Si surface. Since it was for optical experiment, we did not need to go through a standard RCA cleaning, which applied to electrical properties characterization discussed in Chapter 4.

Ag films were prepared with RF magnetron sputtering. After cleaning, the wafer was loaded into a deposition chamber with a holding stage which can heat the sample up to 600°C. We used a 2-inch-diameter 4N-purity silver target with 4N-purity Ar gas for sputtering. The base pressure of the chamber was 2.5×10^{-4} Torr, and the deposition was operated at 5×10^{-3} Torr Ar ambient. After setting up the stage and sealing the chamber, the pumps started to reduce the pressure. The holding stage was heated up to 550°C after the pressure inside the chamber reached the base pressure and stabilized for 10 min. Then the plasma was ignited and stabilized for 10 min with a shutter closed. The deposition rate of Ag was about 0.2 nm/s when RF power was set to 10 W/cm², and the thickness of epitaxial Ag was controlled by deposition time. After sputtering, the sample was taken out of the chamber when its temperature fell **to room temperature**. The key parameters in RF sputtering can be referred from table 3.1.

Table 3.1 Sputtering condition of samples for optical characterization

Target	Ag
Gas	Ar
Temperature/°C	550
Pressure/ mTorr	5.0
Power/ W-cm ⁻²	10
Deposition rate/ nm(s ⁻¹)	~0.2

3.1.2 Angular dependence of reflection characterization

Figure 3.1 shows the experiment set-up to measure the angular dependence of reflection. We use a single wavelength He-Ne laser ($\lambda = 633 \text{ nm}$) as light source, whose beam diameter is 1mm and output power about 8 mW. The sample is fixed on a holder which can be rotated to adjust the incident angle of the laser beam. To clearly define the sign of angle, we define that the positive angle means clockwise direction and the negative angle refers to counterclockwise direction. By rotating the laser around the longitudinal axis, we can test reflection of both TE and TM mode. A germanium optical detector (LM-2) was used to measure the power of reflected beam at the far field and the result can be obtained from an optical power meter connected to the detector.

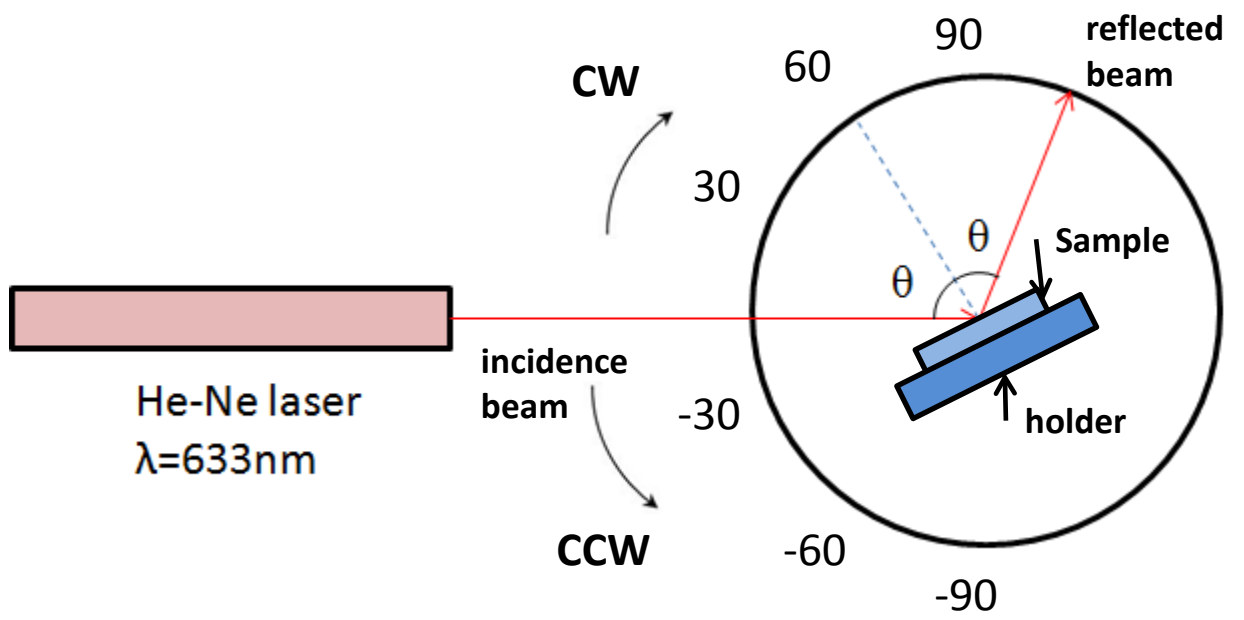


Figure 3.1 Scheme of optical characterize system setup to measure angular dependence of reflection

3.2 EXPERIMENTAL RESULT

3.2.1 Results of bare crystalline silicon substrate

From Fresnel's equation shown below [14]:

TE (s wave) Mode:

$$r_s = \frac{n_1 \cos \theta_i - n_2 \cos \theta_t}{n_1 \cos \theta_i + n_2 \cos \theta_t} \quad (3.2-1)$$

TM (p wave) Mode:

$$r_p = \frac{n_1 \cos \theta_t - n_2 \cos \theta_i}{n_1 \cos \theta_t + n_2 \cos \theta_i} \quad (3.2-2)$$

we can obtain the reflectance that a laser beam incident from air to silicon at a given incident angle by square the reflectivity. For normal incidence case ($\theta_i = 0$), the reflectance given by:

$$R_s = R_p = \left(\frac{n_1 - n_2}{n_1 + n_2} \right)^2 \quad (3.2-1)$$

At 300 K, the refractive index of silicon at 633 nm wavelength is 3.87 [15]. From (3.2-1), we have

$$R = \left(\frac{1 - 3.87}{1 + 3.87} \right)^2 = 0.35 \quad (3.2-2)$$

Also, we can calculate the Brewster's angle [14]:

$$\theta_B = \tan^{-1} \frac{n_2}{n_1} = \tan^{-1} \frac{3.87}{1} = 75.5^\circ \quad (3.2-3)$$

Figure 3.2 shows the angle-dependent reflectance of crystalline silicon. From the figure we can obtain that the reflectance is about 0.35 at normal incidence and the Brewster's angle is about 75. These results match with the theoretical results very well.

Reflectance: Crystalline Silicon

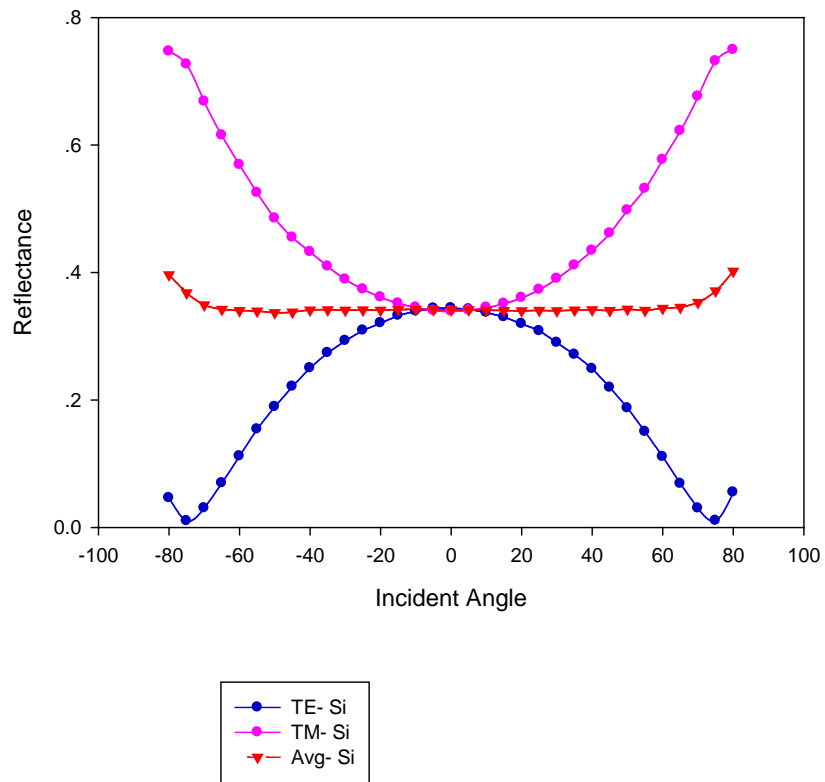


Figure 3.2 Angel-dependent reflectance of crystalline silicon at 633nm wavelength.

3.2.2 Results of epitaxial Ag covered silicon substrate

Typically, the reflection of silicon substrate would increase dramatically if the substrate surface is covered with a thick Ag film. However, our results indicate that if the thickness of film is about 10 nm, the increment of reflection might be inconspicuous. We fabricated samples with different Ag thicknesses varied from 7 nm to 40 nm on silicon and performed angular dependence of reflection characterization. Figure 3.3 to 3.9 show the results of each sample. These results have some similarities with the results obtained from pure silicon (shown in Figure 3.2). First, the average reflectance is almost flat when incident angle is between -70° to 70° . Second, The Brewster's angles are nearly 75° . Also, for samples with an Ag film whose thickness is less than 15nm, the reflectance around normal incident angle is less than 40% and close to 35%.

To compare the average reflectance result at thin Ag thickness condition, we plot some of the results in Figure 3.10, including data from samples whose Ag film is thinner than 15nm. From this figure we find that the reflectances of samples which deposit epitaxial Ag film are close to bare silicon results. Even Ag thickness increase to 15nm, the reflectance increment is only 4% at normal incidence and 2% at 45° to 60° . With Ag film coated, the samples show less reflected at 45° to 60° than at normal incidence. Also, the reflectance shows an increase tendency when the thickness of Ag film increase.

Figure 3.11 shows the results to study about the thickness effect of Ag film on reflectance at thicker cases. The reflectance increases with the film thickness when it is thinner than 20nm but decreases when the film thickness increases to 40 nm.

The reason why the reflectance decreases when the thickness of film increases beyond 20 nm might be the evolution of morphology and the formation of grain structure which are

reported in previous researches [3]. Figure 3.12 shows the SEM image of epitaxial Ag film on Si deposit for 40 s, 50 s and 60 s. In 40 s case, the surface of film was almost flat with a few Ag nano-islands on the Ag film. The grain size was 30 nm in base width, which indicated that during reflectance characterization the incident light was not likely to be scattered since the grain size was too tiny compared with wavelength of laser beam. When deposition time increased to 50 s, the concentration of nano-islands increased and surface became rougher but no large grain structure formed. At 60 s deposition time condition, the morphology of the film changed dramatically, relatively large grain structures (20-100 nm) were clearly formed. Still, the size of grain was not compatible with wavelength of laser. The estimated thickness of 60 s thickness is 12 nm and from our results, 12 nm Ag film coating would not result in obvious reduction of reflectance. However, further deposition might keep increasing the grain size [4]. For Stranski-Krastanow growth, the curvature of the grain is affected by the surface tension at the two-material interface. When the thickness of film increases, new grains can be referred as grain grown on interface with less substrate components thus the surface strain will change, results in grain size change. Also, the deposition temperature was 550 °C, at which thick Ag film will bow and form nano-islands structure. Literature shows that Ag nano-islands formed on Si which size can be up to 200 nm in the base width [16]. With nano-islands structure formed, the surface became rough and part of the light scatter rather than that of reflected. Such light can be reflected back to the air side or the substrate side. Unfortunately, since the intensity of the scattered light is low, we cannot detect it with the detector.

For Photo-Voltaic application, 10 to 15 nm-thick films might be a good choice for surface coating to take advantage of the electrical properties of the film, which will be characterized in Chapter 4, or to induce surface plasmon effect, since no significant increase of

reflection found. In some cases, it might be useful to coat device with about 40 nm-thick films since it induce more scattering and might results in more light absorption in the device, however, such scattering was not characterized so we cannot determine whether it can reduce the total intensity of light that reflected and scattered back to the air.

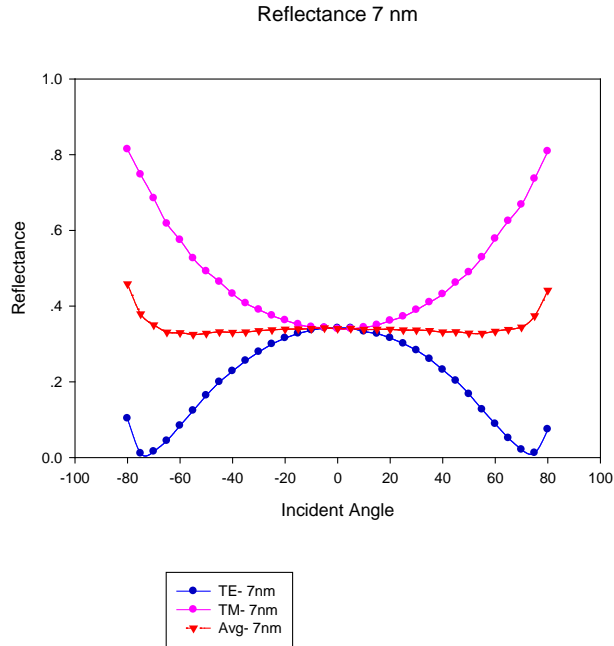


Figure 3.3 Angle-dependent reflectance of crystalline silicon with 7 nm epitaxial Ag covered at 633 nm wavelength

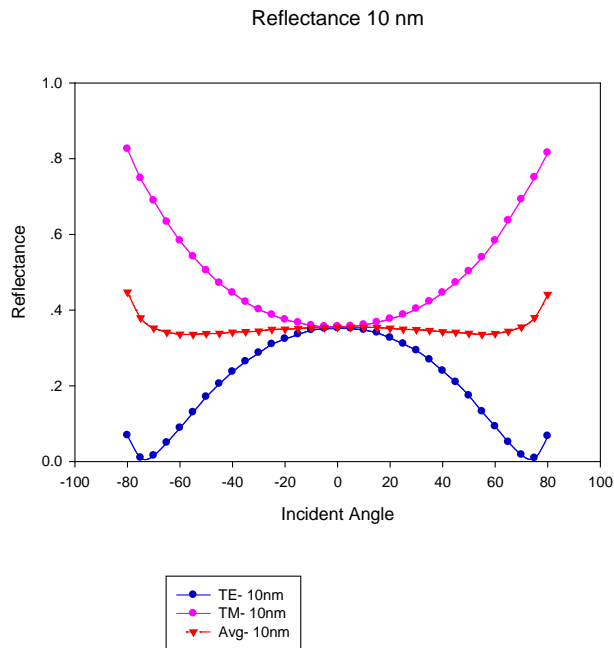


Figure 3.4 Angle-dependent reflectance of crystalline silicon with 10 nm epitaxial Ag covered at 633 nm wavelength

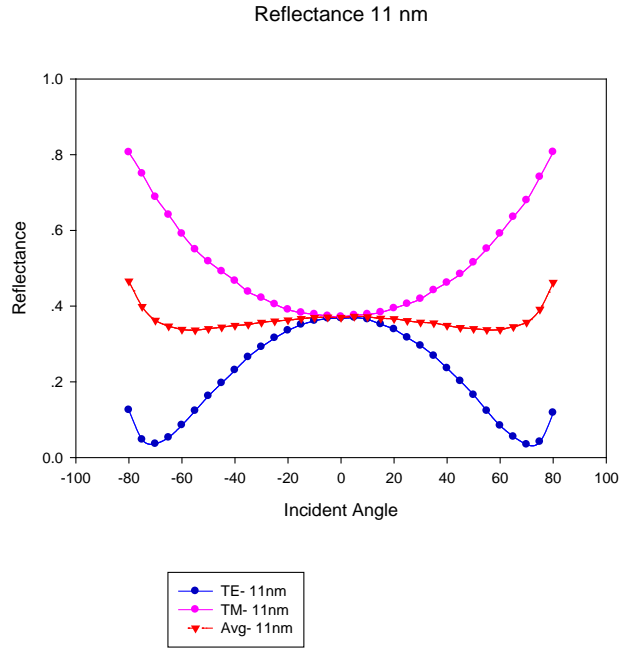


Figure 3.5 Angle-dependent reflectance of crystalline silicon with 11 nm epitaxial Ag covered at 633 nm wavelength

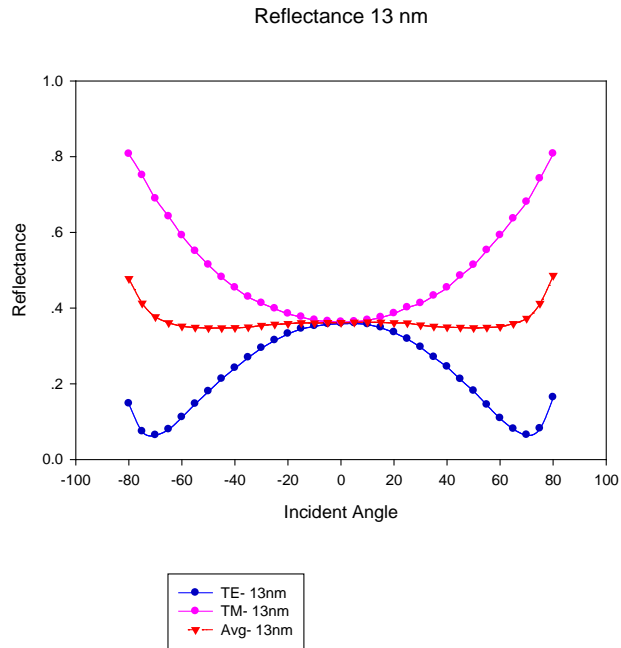


Figure 3.6 Angle-dependent reflectance of crystalline silicon with 13 nm epitaxial Ag covered at 633 nm wavelength

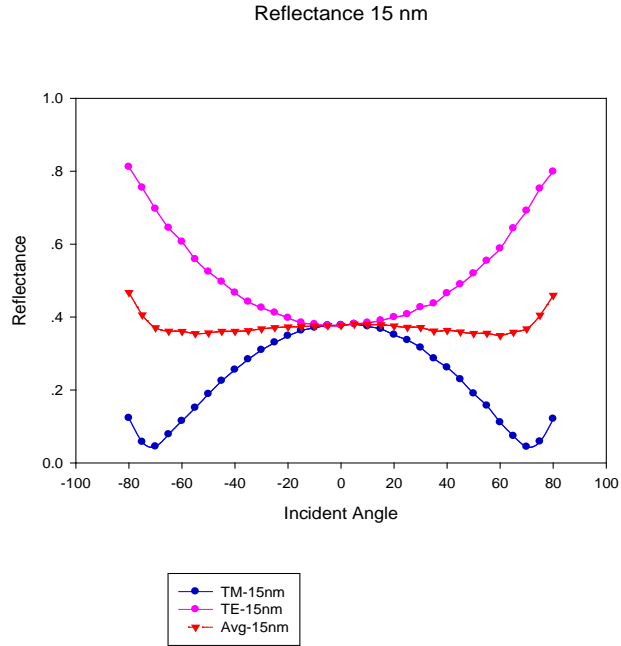


Figure 3.7 Angle-dependent reflectance of crystalline silicon with 15 nm epitaxial Ag covered at 633 nm wavelength

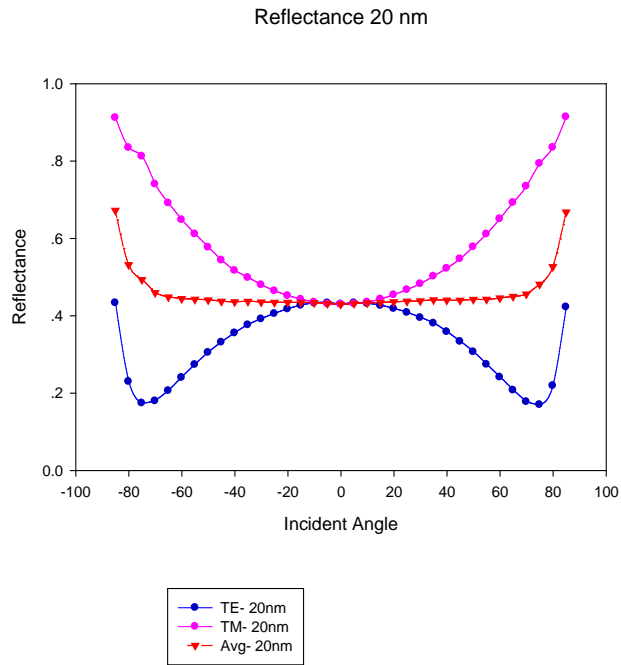


Figure 3.8 Angle-dependent reflectance of crystalline silicon with 20 nm epitaxial Ag covered at 633 nm wavelength

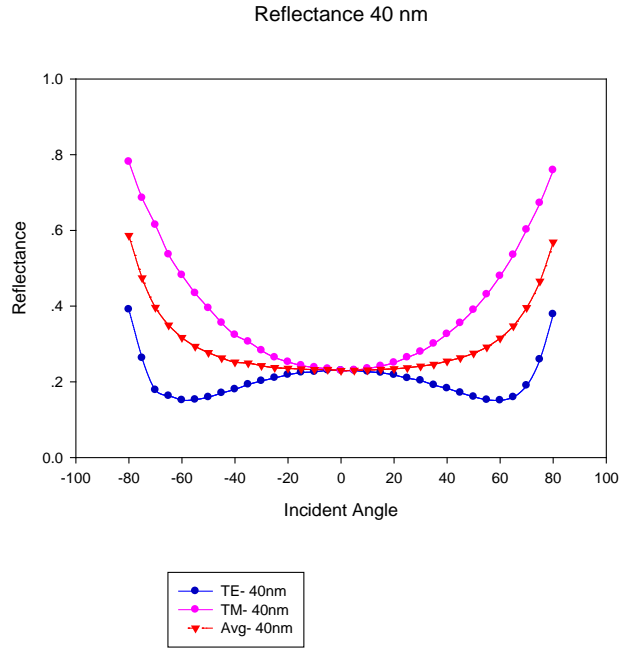


Figure 3.9 Angle-dependent reflectance of crystalline silicon with 40 nm epitaxial Ag covered at 633 nm wavelength

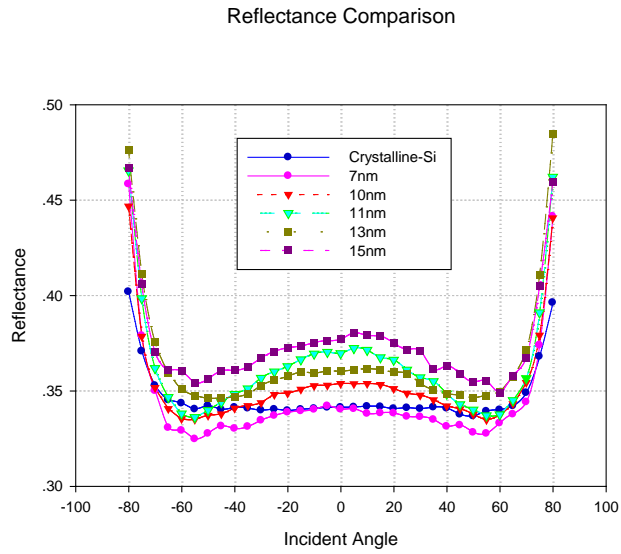


Figure 3.10 Comparison of angle-dependent average reflectance of crystalline silicon with epitaxial Ag (0-15 nm) covered at 633 nm wavelength

Reflectance Comparison

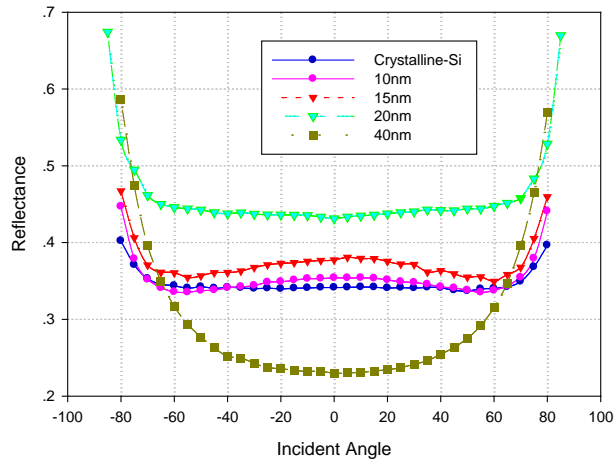


Figure 3.11 Comparison of angle-dependent average reflectance of crystalline silicon with epitaxial Ag (0-40 nm) covered at 633 nm wavelength

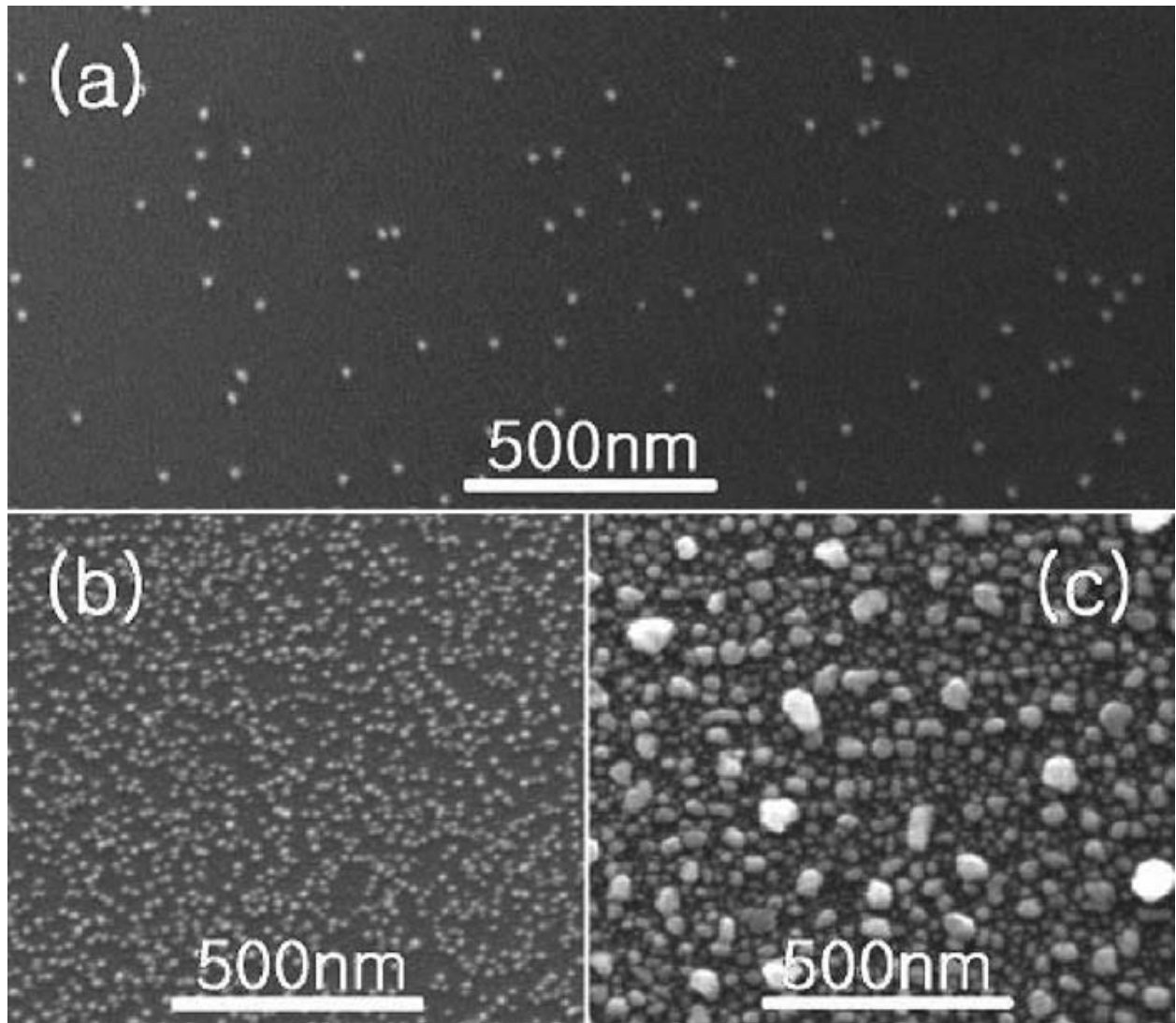


Figure 3.12 SEM image of epitaxial Ag films on Si deposit for (a) 40 s, (b) 50 s and (c) 60 s [3].

4.0 ELECTRICAL PROPERTIES CHARACTERIZATION

Electrical property plays a key role in the application of thin metal film. Typically, we need to understand the conductivity of the material and also the metal-semiconductor contact characteristics. In Chapter 3 we characterized the optical properties of our epitaxial Ag on Si. We found that when the thickness of film on Si substrate is within 10-15 nm range the reflectance will have negligible increment, which meets the requirement of some applications, such as Photo-Voltaic devices. In this chapter we will focus on films with 10-15 nm and study the film conductivity as well as Ag-Si contact. As reference, Al-Si contact will be investigated as well to make a comparison between our epitaxial Ag-Si contact and conventional metal-semiconductor contact which is widely applied nowadays.

4.1 EXPERIMENTAL SETUP

4.1.1 Epitaxial Ag preparation

In our experiments we mostly use p-type Si (001) wafer (substrate resistivity: 10 ± 5 ohm-cm) as substrate. The wafer was cut into 2 cm by 4 cm approximately for deposition substrate. The Si wafer was first degreased with Trichloroethylene for 10 min and then rinsed with DI water. After being degreased, the substrate was cleaned with solvents (acetone, and methanol for 10 min,

respectively) in an ultrasonic bath. After being ultrasonically rinsed, the sample was transferred into deionized (DI) water and rinsed for 2 min. A standard RCA cleaning is processed and after all, it is blown dry with nitrogen gas. After cleaning the native oxide on Si surface was still remain for sputtering process.

The sputtering conditions were the same as described in Chapter 3, which is for optical characterization samples preparation. In our experiment this thickness was set between 10-15 nm and the deposition time is about 1 min. After epitaxial layer sputtering, the sample was performed another sputtering in room temperature to form a thick metallic Ag layer as electrodes, for the purpose of making highly conductive electrodes. The thickness of the metallic Ag is 60 nm. Such structure is shown in Figure 4.1. For samples using shadow mask for patterning, a shadow mask was covered on the substrate. The design of mask is shown in Figure 4.2. The key parameters in RF sputtering can be referred from table 4.1.

Table 4.1 Sputtering Condition of samples for electrical characterization

Target	Ag
Gas	Ar
Temperature/ °C	550 (epitaxial)/R.T. (metallic)
Pressure/ mTorr	5.0
Power/ W-cm ⁻²	10
Deposition rate/ nm(s ⁻¹)	~0.2 (epitaxial)/~0.5 (metallic)

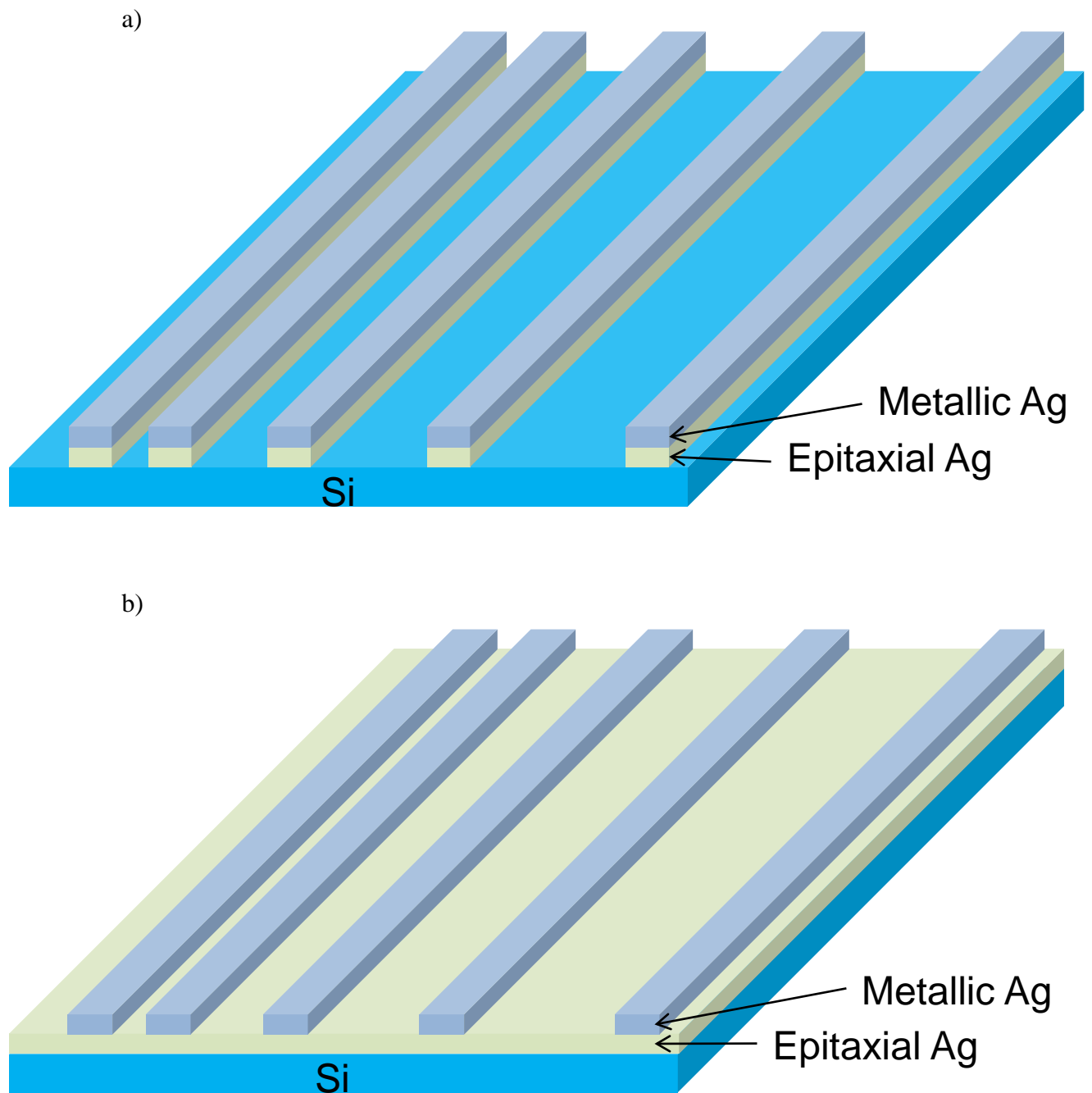


Figure 4.1 Structure of prepared samples in electrical characterization. a) Discrete epitaxial Ag sample is for study of contact resistivity and b) continuous sample is for study of epitaxial Ag conductivity

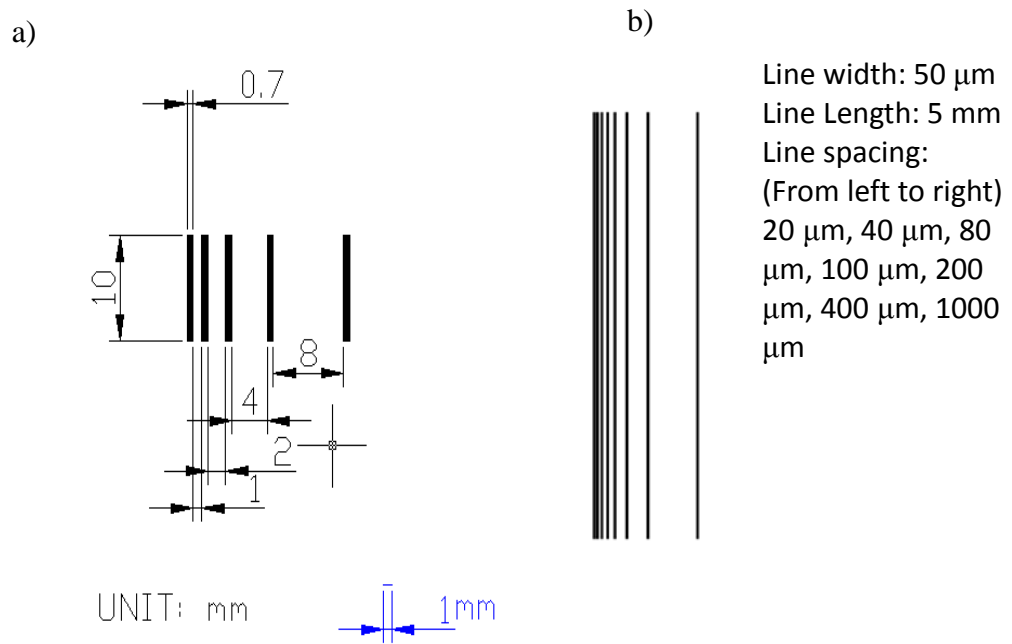


Figure 4.2 mask pattern design. a) mm scale mask (available in shadow mask and lithography mask). b) μm scale mask (available in lithography mask only)

Al was deposited on Si to make reference samples. We use the same substrate which was using in Ag sputtering. To make good ohmic contact, native oxide was removed by dilute HF (HF(49%)+DI H₂O in vol. ratio 1:30) for 20 s. After rinsed with DI water, the samples were blown dry with nitrogen. Besides using shadow mask for patterning, we process Al-Si samples with photolithography in most of the cases. A positive photoresist (PR) (Shipley 1827) was spin-coated on the substrates at 3000 rpm for 30 s, which formed 3 μm thick PR. Then the silicon substrates were baked in 90 °C for 30 min. The samples were then processed to expose for 12 min and developed in Shipley 351 developer which is dilute by DI water in volume ratio 1:4. After exposure the samples were processed to thermal evaporation. The base pressure of the evaporation is 9×10^{-5} Torr, and 100 nm Al was deposited on the samples. Finally, PR was removed by acetone at room temperature and ohmic contact annealing was performed at 450 °C for 30 min in forming gas (N₂/H₂ = 90%/10%). The key parameters are shown in table 4.2 and 4.3.

Table 4.2 Photolithography Condition for TLM patterning

PR	Shipley 1827
Spin coat speed/ rpm	3000
Spin coat Time/ s	30
Thickness/ μm	~ 3
Expose Time/ min	12
Developing Time/ min	3
Developer	Shipley 351 : DI- H_2O (1:4)
PR remover	Room temperature acetone

Table 4.3 Thermal Evaporation Condition for Al deposition

Source	Al
Time/ min	13
Thickness/ nm	100
Chamber pressure/ Torr	9×10^{-5}
Deposit rate/ nm/s	~ 0.13

4.1.2 Contact resistivity characterization using TLM analysis

In Chapter 2 we discussed the characterization method of TLM analysis and derived the formula. We measure the total resistance between each pair of adjacent electrodes and plot the curve distance of versus resistance between electrodes. From (2.2-14), (2.2-15) and (2.2-16) we know that the final result is as below:

$$L_T = R_c / k \quad (4.1-1)$$

$d > 1.2 \times L_T$:

$$\rho_c = R_c L_T w \quad (4.1-2)$$

$d < 1.2 \times L_T$:

$$\rho_c = R_c d w \quad (4.1-3)$$

where R_c is the contact resistance obtained from the intercept of R axis in R-L curve, w is the length of electrodes and k is the slope of curve. The electrode pattern and the R-L curve illustration are shown in Figure 2.3 in Chapter 2, with some of the important parameters indicated.

We used HP 4145B Semiconductor Parameter Analyzer to measure the I-V curve of each pair of adjacent electrodes. The electrode was contact with probe which was connected with the analyzer. From the curve we can determine whether the contact is ohmic by observing whether the curve is linear and reading the resistance from the inverse of the slop of I-V curve.

4.2 EXPERIMENT RESULT AND DISCUSSION

4.2.1 Epitaxial Ag-Si contact resistivity

4.2.1.1 Ag samples using mm scale pattern on medium doped substrate To measure the Ag-Si contact resistivity, we chose p-type Si(001) wafer (substrate resistivity: 10 ± 5 ohm-cm, defined as medium doped substrate) as substrate and did patterning with mm scale pattern shadow mask as show in figure 4.1 a) and 4.2 a). For reference Al-Si contact samples were also prepared. The results are shown in figure 4.3 and table 4.4.

From the results we can see that the contact resistivity of Ag-Si was about 1 ohm-cm², while the Al-Si contact was 0.250 ohm-cm². The measured substrate resistivity was all within the range of nominal value (10 ± 5 ohm-cm) which suggests that the results were effective and consistent. From our measurement the contact resistivity of Ag-Si was about 5 times of that for Al-Si, which suggests that our epitaxial Ag-Si was not as good as but still compatible with conventional Al-Si contact.

However, it was reported that the Al-Si contact at this range is about 10^{-2} ohm-cm², which is much lower than the results we got [8]. The reason might be that the mask we used is mm scale mask but typical TLM analysis prefer μm scale mask (typically 10-100 μm). To exam the mask size effect, we fabricated samples with μm scale pattern. However, the μm pattern can only be achieved by photolithography.

To make sure that switching from shadow mask to photolithography will not significantly change the results, we made another sample which did not use the mm scale pattern but photolithography mask. The result is shown in figure 4.3 and table 4.4. The substrate resistivity

Table 4.4 Result of contact resistivity characterization for epitaxial Ag-Si and Al-Si reference
(shadow mask, mm scale, substrate: medium doped)

	Ag-Si (epitaxial Ag thickness = 11nm, shadow mask)	Ag-Si (epitaxial Ag thickness = 15nm, shadow mask)
Intercept = $2R_c$ / ohm	38.2	29.48
Slope (k) / ohm/mm	25.54	21.10
regression coefficient	0.992	0.998
Contact resistance (R_c) / ohm	19.1	14.74
Substrate resistivity / ohm-cm	13.39	11.08
Contact resistivity / ohm-cm ²	1.34	1.03
	Al-Si (shadow mask)	Al-Si (photolithography mask)
Intercept = $2R_c$ / ohm	18.54	25.74
Slope (k) / ohm/mm	27.55	21.37
regression coefficient	0.999	0.998
Contact resistance (R_c) / ohm	9.270	12.87
Substrate resistivity / ohm-cm	11.57	11.22
Contact resistivity / ohm-cm ²	0.250	0.775

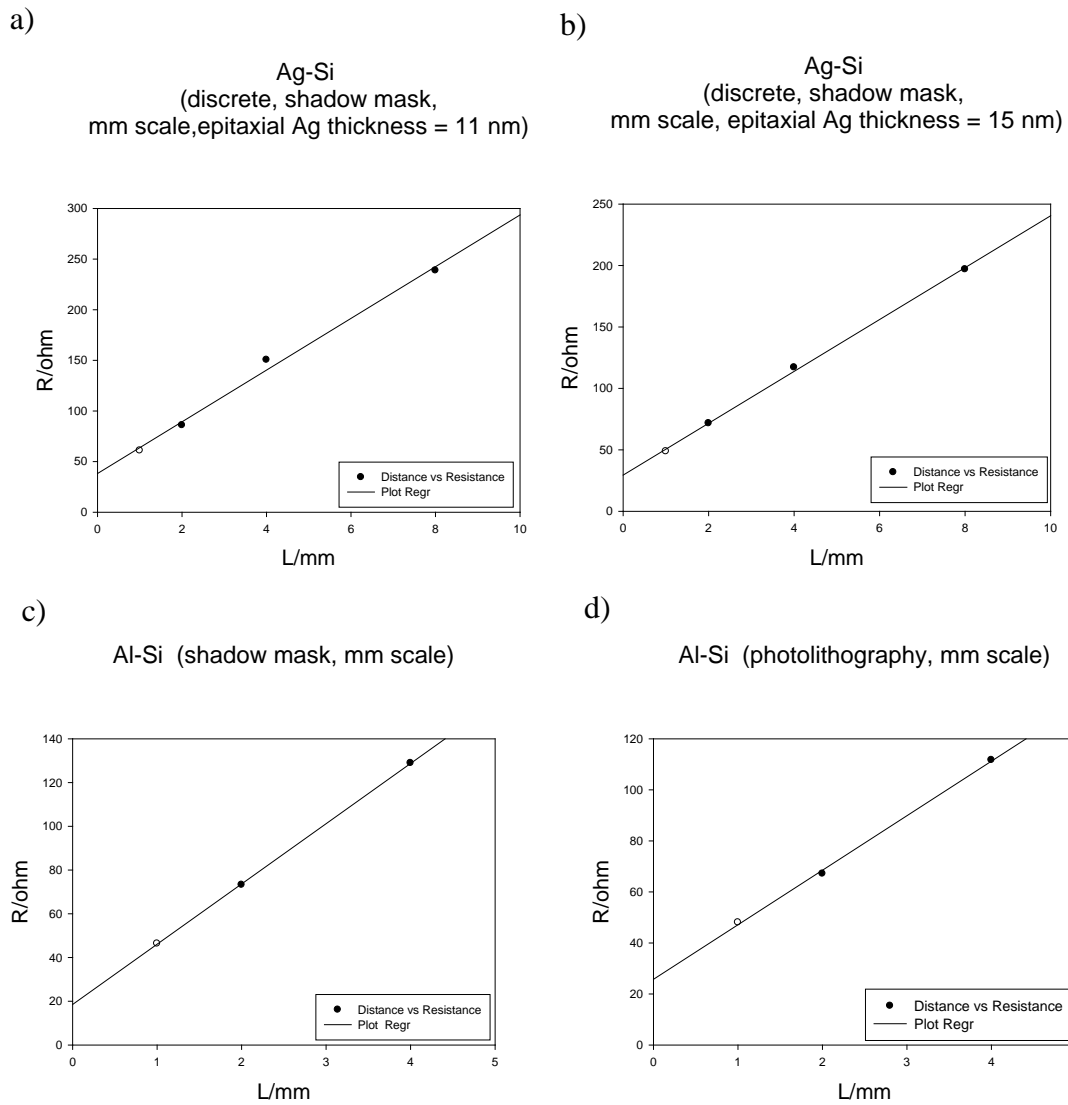


Figure 4.3 R-L curves: a, b) Ag-Si samples patterned by shadow mask with mm scale pattern and discrete epitaxial Ag layer. c) Al-Si samples patterned by same shadow mask. d) Al-Si samples patterned by photolithography mask which has the same pattern as shadow mask used in previous samples

did not change much, which confirms that the measurement was effective, but the contact resistivity increased from 0.250 ohm-cm^2 to 0.775 ohm-cm^2 . Still, the order of magnitude remains the same, so we can conclude that changing patterning method would not significantly affect the results.

4.2.1.2 Ag samples using μm scale pattern on medium doped substrate For Al-Si reference samples, switching from shadow mask to photolithography is not difficult. Nevertheless for Ag-Si sample, lift-off cannot be processed by sputtering with 550°C because PR cannot survive. Therefore the only way to process Ag with μm scale mask is to deposit the planar film first on substrate and then etch pattern with chemical. The lithography process was similar to that described earlier this chapter, but before processing to chemical etching we needed to hard bake the samples in 110°C for 30 min. After hard baking, the samples were etched in dilute nitride acid (HNO_3 : DI water, 1:2 in volume ratio) for 20 s. The Ag films in the area not covered with PR were completely removed. PR was removed by acetone at room temperature after etching. The results are shown in figure 4.4 and table 4.5.

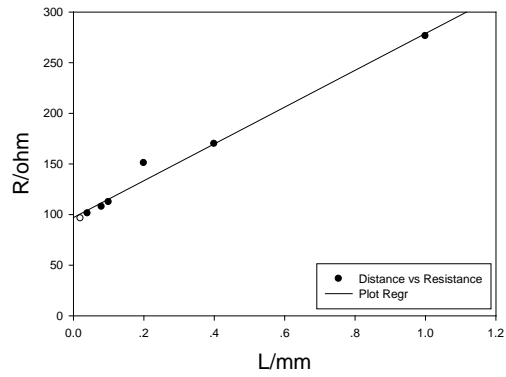
From the results we can see that the contact resistivity of Ag-Si was 0.121 ohm-cm^2 , while for Al-Si contact it was 0.0570 ohm-cm^2 . Compared with previous mm scale mask results (about 1 ohm-cm^2 and 0.250 ohm-cm^2 , respectively), the results from μm scale mask reduced 5 to 8 times which is close to one order of magnitude difference. Also, the Al-Si results were met the reported 10^{-2} ohm-cm results [8]. We believe that this result correctly reflects the contact resistivity in both cases.

Table 4.5 Result of contact resistivity characterization for epitaxial Ag-Si and Al-Si reference
(photolithography mask, μm scale, substrate: medium doped)

	Ag-Si (epitaxial Ag thickness = 11 nm)	Al-Si
Intercept = $2R_c$ / ohm	97.11	45.56
Slope (k)/ ohm/mm	181.8	163.9
regression coefficient	0.985	0.997
Contact resistance (R_c)/ ohm	48.55	22.78
Substrate resistivity/ ohm-cm	47.72	43.01
Contact resistivity/ ohm-cm ²	0.121	0.0570

a)

Ag-Si
(discrete, photolithography,
 μm scale, epitaxial Ag thickness = 11 nm)



b)

Al-Si (photolithography, μm scale)

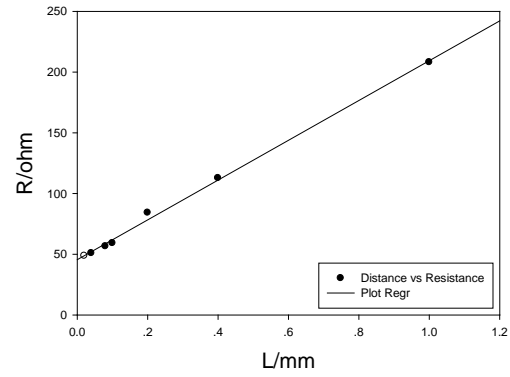


Figure 4.4 R-L curves: a) Ag-Si samples patterned by photolithography mask with μm scale pattern and discrete epitaxial Ag layer. b) Al-Si samples patterned by same by photolithography mask.

However, the measured substrate resistivity was about four times higher than the nominal value. This might be explained as following: The thickness of the wafer is 525 μm , which is larger than most of the distance between electrodes we tested in the experiments. Generally, the current will always tend to go through the path with least resistance, thus most of the current will be conducted by the surface of the wafer. However, when we calculated the equivalent substrate resistivity, we assumed that the current was evenly distributed. If we assume sheet resistance of Si substrate was the same with the nominal value, we can calculate the depth that current transmit in substrate. Assume the nominal value is 10 ohm-cm and the current is evenly distributed within this depth:

$$H_{equ} = H_{nom} \frac{\rho_{nom}}{\rho_{measured}} = 525 \frac{10}{45} = 117 \mu\text{m} \quad (4.2-1)$$

where H_{equ} is the equivalent depth that current pass through, H_{nom} is the nominal thickness of wafer, ρ_{nom} is the nominal substrate resistivity and $\rho_{measured}$ is the measured substrate resistivity. Since H_{equ} is within the same order of magnitude with the distances we tested, we believe that it supports our assumption which explains the abnormal substrate resistivity results.

4.2.1.3 Ag samples using mm scale pattern on highly doped substrate In Chapter 2 we discussed how substrate doping will affect the contact resistivity. To prepare such substrate, an n^+ -doped layer was prepared on p-type Si (001) wafer (substrate resistivity: $10 \pm 5 \text{ ohm-cm}$). The n-dopant (PhosPlus TP-470, TECHNEGLAS) was diffused at $1000 \text{ }^\circ\text{C}$ for 45 min. The expected junction depth was approximately $3 \mu\text{m}$. After diffusion, a phosphors glass layer was formed on the surface and removed by diluted HF acid (HF: DI water, 1:10 in volume ratio) for 2 min.

Ag-Si
(discrete, shadow mask, mm scale,
highly doped substrate, epitaxial Ag thickness = 11 nm)

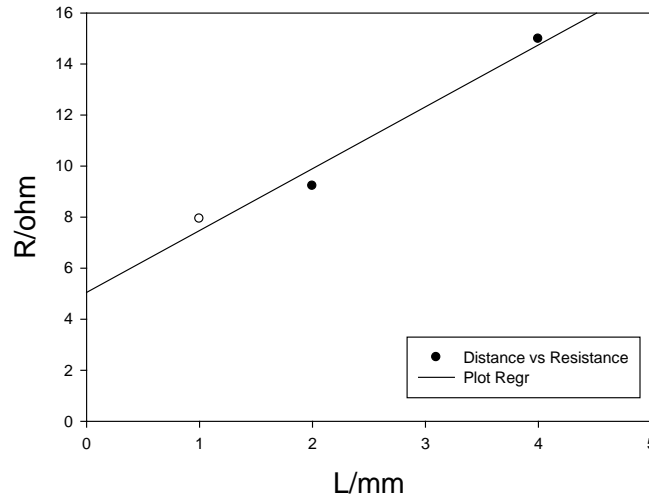


Figure 4.5 R-L curves: Ag-Si samples patterned by shadow mask with mm scale pattern and discrete epitaxial Ag layer on highly doped substrate.

Table 4.6 Result of contact resistivity characterization for epitaxial Ag-Si and Al-Si reference (photolithography mask, mm(Ag)/ μm (Al) scale, substrate: highly doped)

	Ag-Si (epitaxial Ag thickness = 11 nm)
Intercept = $2R_c$ / ohm	5.051
Slope (k)/ ohm/mm	2.425
regression coefficient	0.974
Contact resistance (R_c)/ ohm	2.576
Substrate resistivity/ ohm-cm	0.144
Contact resistivity/ ohm-cm ²	1.34

For Ag-Si contact we used mm-scale shadow mask and the results is shown in figure 4.5 and table 4.6. Due to substrate size the width of electrode on this sample is 8 mm rather than 10 mm. From the result we learned that the contact resistance was reduced to 0.144 ohm-cm² from 1.34 ohm-cm², which confirmed that the contact resistivity will reduce if the doping level of substrate increases. Considering the mask effect to TLM test, the actual contact resistance might be one order of magnitude lower than this result.

Table 4.7 shows the summary of experiment results about the contact resistivity of our epitaxial Ag film on Si. From the results we learned that under the same substrate condition, the contact resistivity of epitaxial Ag on Si is 3 to 5 times higher than Al on Si. It shows that our epitaxial Ag-Si contact is compatible with, although not as good as, conventional Al-Si contact. Also, increasing the doping level of substrate can reduce the contact resistivity, which is explained theoretically in Chapter 2.

Table 4.7 Summary of experiment result for epitaxial Ag film on Si

Ag film thickness	Pattern Scale	Substrate	Contact resistivity of Epitaxial Ag on Si	Al (reference)
11nm	mm scale	Medium doped	1.34 ohm-cm ²	0.250 ohm-cm ²
15nm	mm scale	Medium doped	1.03 ohm-cm ²	
11 nm	μm scale	Medium doped	0.121 ohm-cm ²	0.0570 ohm-cm ²
11nm	mm scale	Highly doped	0.144 ohm-cm ²	N/A

It was reported that Al-Si contact resistivity is related to post-metallization annealing temperature, because during annealing a thin metal-semiconductor alloy formed which would be beneficial to form ohmic contact [10]. When annealing temperature increases, such thin alloy would be formed easier thus results in better ohmic contact (low contact resistivity). Figure 4.6 shows the phase diagram of Ag-Si and Al-Si material systems [17]. From the phase diagram we learned that Al-Si alloy formed at 850 K (577°C), while Ag-Si alloy formed at 1100 K (827°C), and typical annealing temperature for Al is 450°C or above [10] and for Ag is about 780°C or above [11]. However, our Ag sputtering temperature is 550°C, which is much lower than 780°C. This suggests us that our Ag sputtering method might be a better way to form Ag-Si contact, and also infers that we might achieve lower contact resistivity if we increase the sputtering Temperature.

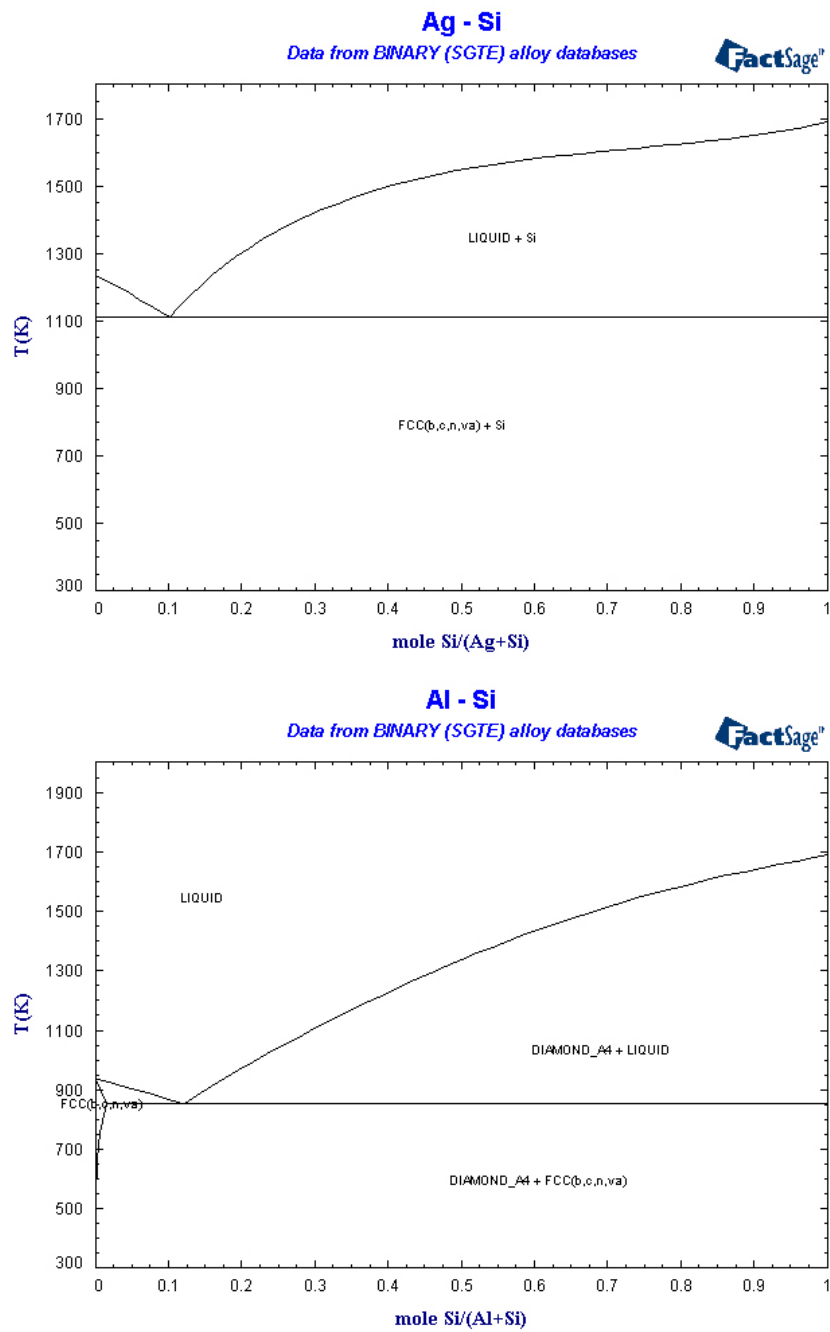


Figure 4.6 Phase diagram of Ag-Si and Al-Si material system [17]

4.2.2 Epitaxial Ag resistivity

To measure the epitaxial Ag resistivity, we chose p-type Si (001) wafer (substrate resistivity: 10 ± 5 ohm-cm) as substrate and did patterning with mm scale pattern shadow mask as figure 4.1 b) and 4.2 a). In this case, when we measure the total resistance between electrodes, epitaxial Ag film also serves as conductor which can be consider parallel to the substrate. Therefore we can calculate the sheet resistance of Ag film as follow:

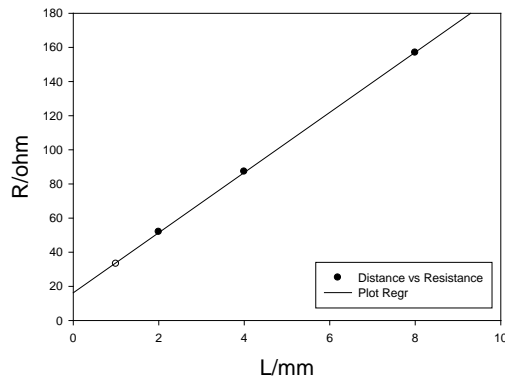
$$R_{Ag} = \frac{R_{total} R_{sub}}{R_{sub} - R_{total}} \quad (4.2-2)$$

Where R_{total} is the substrate sheet resistance we calculate from samples with continuous Ag film and R_{sub} is the substrate sheet resistance with discrete Ag film. The results are shown in figure 4.7 and table 4.8.

We studied the same issue using μm scale pattern photolithography mask as well. However, lift-off was used in such experiments. We first deposited an epitaxial Ag layer by sputtering first, and then did photolithography and deposited metallic Ag with thermal evaporation. The photolithography-evaporation-liftoff process was the same as described for Al patterning earlier this chapter and no post deposition annealing was needed in this case. The results are shown in figure 4.8 and table 4.9. Results show that the sheet resistance for 11 nm thick Ag is about 250~570 ohm, which means the material resistivity is about $2.75\sim 6.25\times 10^{-4}$ ohm-cm. For 15 nm thick Ag the sheet resistance is about 1500 ohm, which has the corresponding material resistivity of 2.25×10^{-3} ohm-cm. However, the substrate resistivity for continuous epitaxial Ag samples is nearly the same (176.2 ohm and 186.3 ohm for 11 nm and 15

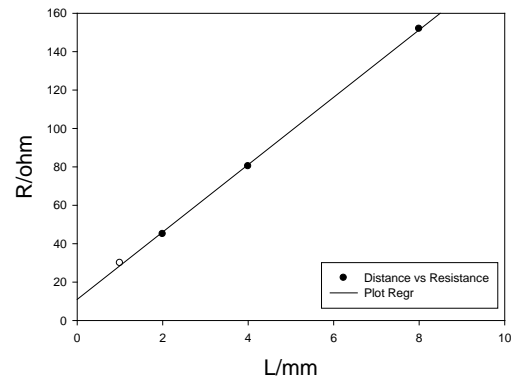
a)

Ag-Si
(continuous, shadow mask,
mm scale, epitaxial Ag thickness = 11 nm)



b)

Ag-Si
(continuous, shadow mask,
mm scale, epitaxial Ag thickness = 13 nm)



c)

Ag-Si
(continuous, shadow mask,
mm scale, epitaxial Ag thickness = 15 nm)

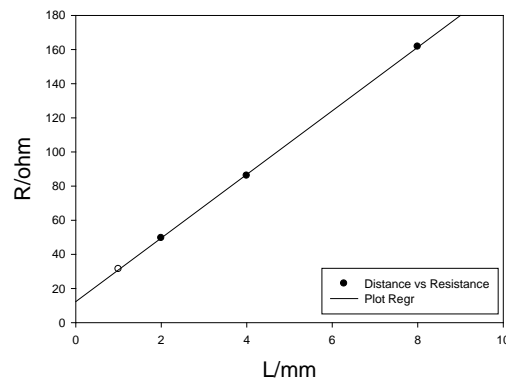


Figure 4.7 R-L curves: Ag-Si samples patterned by shadow mask with mm scale pattern and continuous epitaxial Ag layer on medium doped substrate.

Table 4.8 Result of substrate sheet resistance characterization for epitaxial Ag-Si
(shadow mask, mm scale, substrate: medium doped)

	Ag-Si (continuous epitaxial Ag, thickness = 11 nm)	Ag-Si (continuous epitaxial Ag, thickness = 15 nm)
Intercept ($2R_c$) /ohm	16.2	12.31
Slope (k) /ohm/mm	17.62	18.63
regression coefficient	0.999	0.999
Substrate sheet resistance/ohm	176.2	186.3
	Ag-Si (discrete epitaxial Ag, thickness = 11 nm)	Ag-Si (discrete epitaxial Ag, thickness = 15 nm)
Intercept ($2R_c$) /ohm	38.2	29.48
Slope (k) /ohm/mm	25.54	21.10
regression coefficient	0.992	0.998
Substrate sheet resistance/ ohm	255.4	211.0
Epitaxial Ag sheet resistance/ ohm	568.2	1591

Ag-Si
(continuous, photolithography,
um scale, epitaxial Ag thickness= 11 nm)

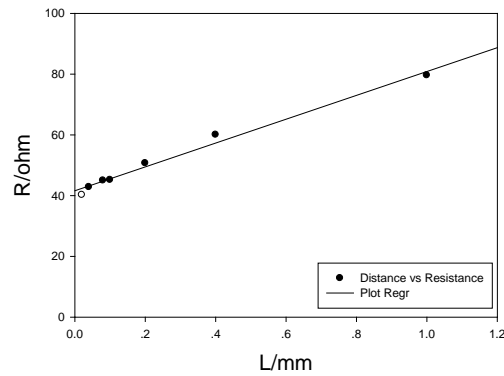


Figure 4.8 R-L curves: Ag-Si samples patterned by photolithography mask with μm scale pattern and continuous epitaxial Ag layer on medium doped substrate.

Table 4.9 Result of substrate sheet resistance characterization for epitaxial Ag-Si (photolithography μm scale, substrate: medium doped)

	Ag-Si (continuous epitaxial Ag, thickness = 11 nm)
Intercept ($2R_c$) /ohm	41.62
Slope (k) /ohm/mm	39.25
regression coefficient	0.9865
Substrate sheet resistance/ohm	196.3
	Ag-Si (discrete epitaxial Ag, thickness = 11 nm)
Intercept ($2R_c$) /ohm	97.11
Slope (k) /ohm/mm	181.8
regression coefficient	0.985
Substrate sheet resistance/ ohm	909.9
Epitaxial Ag sheet resistance/ ohm	250.3

nm, respectively), which might suggest that increasing the thickness of epitaxial Ag would not help increase the sheet resistance of the Ag film.

To investigate such issue, we tested an additional condition that the Ag film thickness is 13nm. The result is shown in table 4.10 and we learned that the substrate sheet resistance stayed almost the same when the film thickness increased from 11 nm to 15 nm. This suggests that our assumption is true and increasing the film thickness would not contribute to current flowing.

Table 4.10 Result of sheet resistance for epitaxial Ag covered Si for film thickness effect
(shadow mask, mm scale, substrate: medium doped)

	Ag-Si (continuous epitaxial Ag, thickness = 11 nm)	Ag-Si (continuous epitaxial Ag, thickness = 13 nm)	Ag-Si (continuous epitaxial Ag, thickness = 15 nm)
Intercept ($2R_c$) /ohm	16.2	11.0	12.31
Slope (k) /ohm/mm	17.62	17.54	18.63
regression coefficient	0.999	0.999	0.999
Sheet resistance/ohm	176.2	175.4	186.3

Figure 4.9 illustrates that the current flows between electrodes. Considering the morphology study results discussed in Chapter 3, we believe that planar Ag film when the thickness of film is thin. Only a few boundaries are formed during this stage and results in higher resistivity of Ag film than bulk Ag material. Grain structure is formed when the thickness of the Ag film increases beyond 10 nm, which means that the top surface of Ag film is not planar. Unlike planar Ag film near the Ag-Si surface, the Ag film near the top surface is not electrically well connected because boundaries of grains occurred serve as barrier, and carrier cannot easily

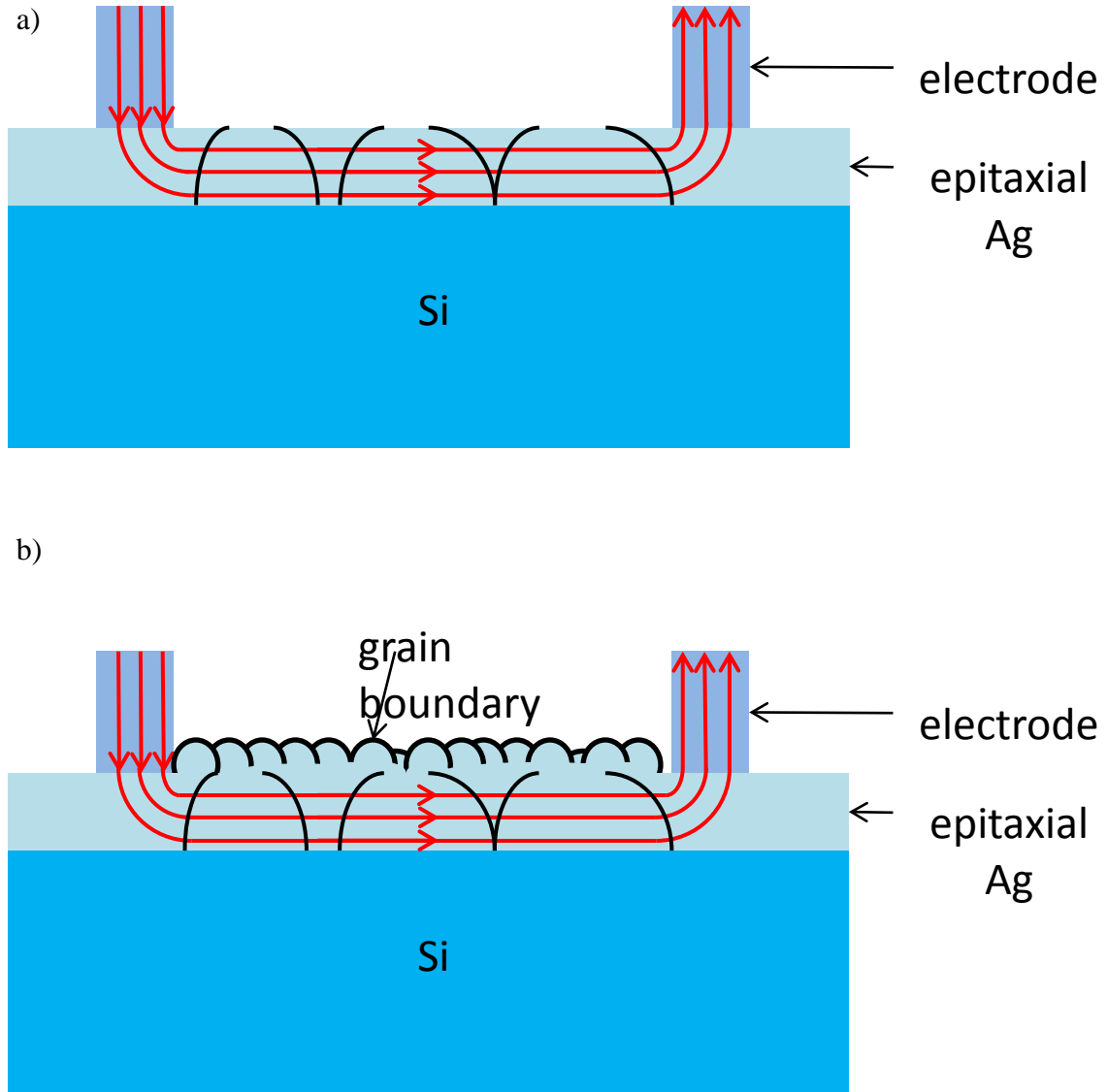


Figure 4.9 Illustration of current flow between electrodes for continuous epitaxial Ag films covered Si. a) Before grain shape surface formed, only sparse boundaries occur in the film b) After grain shape surface formed, the grain structure contributes to increasing the thickness of the film but not the current flow because boundaries of grains serve as barrier to prevent carrier transfer.

transfer between the grains but can only through the underneath Ag film. In this case the current would still being conduct by the part of the Ag film near the Ag-Si surface.

Table 4.11 shows the summary of the results about the Ag film resistivity characterization. For Bulk Ag, the material resistivity is 1.6×10^{-6} ohm-cm, which is about 100-time lower than our results on epitaxial Ag. The reason might be the purity of Ag in the epitaxial Ag film. Figure 4.10 shows the XPS analysis result of an Ag film sputtered for 90 s at 550 °C from previous study in our group about the same kind of Ag film [2]. It shows that besides Ag, O and Si components also occurred in such epitaxial Ag film, which might increase the resistivity of film. Such Si and O component might come from the native oxide layer, substrate or ambient which is not possible to remove completely.

Reports show that coating a current spreading layer, such as indium tin oxide (ITO) or grapheme, might help increasing the efficiency of solar cell [18] [19]. Such current spreading layer can better collect the carriers and reduce the recombination. From our results, thin epitaxial Ag films have the similar properties with these layers. The sheet resistance of grapheme in the report is 1730 ± 600 and 610 ± 140 ohm which is close to our epitaxial Ag films [19]. Thus, such Ag films might be applied to similar applications.

Table 4.11 Summary of experiment result about epitaxial Ag film resistivity on Si

Ag film thickness	Pattern Scale	Substrate	Epitaxial Ag film resistivity
11nm	μm scale	Medium doped	2.75×10^{-4} ohm-cm
11nm	mm scale	Medium doped	6.25×10^{-4} ohm-cm
15nm	mm scale	Medium doped	2.25×10^{-3} ohm-cm

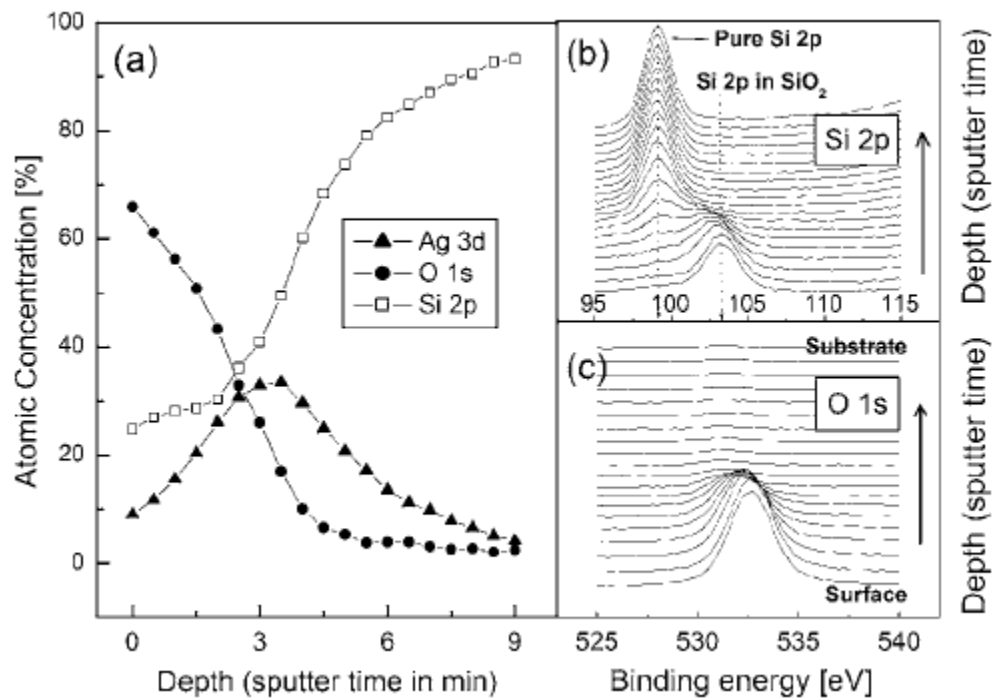


Figure 4.10 XPS analysis results of a Ag film sputtered for 90 s at 550 °C: a) Depth profiles of Ag, O and Si, b) Depth profile of Si 2p energy spectra, c) Depth profile of O 1s energy spectra [2]

5.0 SUMMARY

In this work, we studied the optical and electrical properties of epitaxial Ag deposited on Si by radio-frequency (RF) magnetron sputtering at 550°C. In optical characterization, the results indicated that when film thickness was less than 15 nm, the reflectance of light only increased less than 4% when the incident angle of laser beam was within -70° to 70°. As the thickness of Ag films increased to 40 nm, scattering effect occurs due to large grain structure formed at the surface of Ag films, and reflectance decreased to 25% at normal incident angle. In electrical characterization, we found epitaxial Ag films and substrate Si forms good ohmic contact. When substrate was medium doped, the Ag-Si contact resistivity is about 0.1 ohm-cm². We also confirmed that increased the substrate contact doping level the Ag-Si contact resistivity will decreased. Also, results showed that with epitaxial Ag covered the Si substrate was more conductive since the Ag films served as a current conducting layer. However, thick Ag films would not help conducting the current better than thin films since grain structure boundaries became barriers which prevent carrier transfer between grains. The resistivity of the material from this epitaxial Ag films was about 10⁻⁴ ohm-cm, most likely due to the presence of background impurities such as Si and O.

Such result might suggest that this kind of Ag films might be introduced to photo-voltaic devices. With these Ag films coating the devices, the carriers can be better collected by the Ag films without any increase of reflectance at the surface of device. Also, ohmic contact can be

formed so Ag electrodes can be deposited without 800°C high temperature annealing but with 550°C process temperature. The fabrication process of this kind of Ag film is relatively easy as well, since it requires only a shadow mask for patterning without any additional chemical treatment, such as etching etc. From our results, the optimized film thickness for photo-voltaic devices, which require inducing minimum reflectance increase and good ohmic contact, might be 10-15 nm.

BIBLIOGRAPHY

- [1] Review in V. A. Grazhulis, *Progress in Surface Science* Vol. 36, No. 2, 89 (1991).
- [2] T. B. Hur, H. K. Kim and J. Blachere, *Physical Review B*, Vol. 75, No. 20 205306 (2007).
- [3] T. B. Hur, H. K. Kim, D. Perello, M. Yun, A. Kulovits, and J. Wiezorek, *Journal Of Applied Physics*, Vol 103, No 10, 103507 (2008).
- [4] D. J. Eaglesham and M. Cerullo, *Physical Review Letters*, Vol. 64, No. 16, 1943-1946 (1990)
- [5] D. Winau, H. Itoh, A. K. Schmid, and T. Ichinokawa, *Surface Science* Vol. 303, No. 1-2, 139, (1994).
- [6] In an unpublished report: W. Shockley Air Force Atomic Laboratory, Wright-Patterson Air Force Base, Report No. AL-TOR-64-207, 1964
- [7] H. H. Berger, *Solid-State Electron.* 15 145-158 (1972)
- [8] Dieter K. Schroder and Daniel L. Meier, *IEEE Transaction on Electron Device*, Vol. 31, No. 5, 637-647 (1984)
- [9] F. A. Kroger, G. Diemer, and H. A. Klasens, *Physical Review*, Vol. 103, 279, (1956)
- [10] M. Finetti et al., *Solid-State Electronics*, Vol. 23, No. 3, 255-262 (1980)
- [11] L.M. Porter, A. Teicher and D.L. Meier, *Solar Energy Materials & Solar Cell*, Vol.73, No. 2, 209-219 (2002)
- [12] D. C. Look, *Electrical Characterization of GaAs Materials and Devices*, John Wiley & Sons Press, 1989
- [13] G. K. Reeves and H. B. Harrison, *IEEE Electron Device Letters*, Vol. 3, No. 5, 111-113 (1982)
- [14] A. Yariv and P. Yeh, *Photonics*, Oxford, 2007.

[15] M. A. Green and M. J. Keevers, *Progress in Photovoltaics: Research and Applications*, Vol 3, No. 3, 189 (1995).

[16] M. V. Chursanova, V. M. Dzhagan, V. O. Yukhymchuk, O. S. Lytvyn, M. Ya. Valakh, I. A. Khodasevich, D. Lehmann, D. R. T. Zahn, C. Waurisch and S. G. Hickey, *Nanoscale Research Letters* Vol 5, No. 2, 403-409 (2010)

[17] Binary (SGTE) alloy database

[18] J. P. Shim, S. R. Jeon, Y. K. Jeong, and D.S. Lee, *IEEE Electron Devices Letters*, Vol. 31, No. 10, 1140-1142 (2010)

[19] J. P. Shim, M. Choe, S. R. Jeon², D. Seo, T. Lee, and D. S. Lee, *Applied Physics Express*, Vol. 4, No. 5, 052302 (2011)